
All ETDs from UAB

UAB Theses & Dissertations

2009

Design, Analysis and Deve Lopment of Optimized Thermoplastic Pultruded Profiles

Leigh A. Hudson
University of Alabama at Birmingham

Follow this and additional works at: <https://digitalcommons.library.uab.edu/etd-collection>

Recommended Citation

Hudson, Leigh A., "Design, Analysis and Deve Lopment of Optimized Thermoplastic Pultruded Profiles" (2009). *All ETDs from UAB*. 6783.
<https://digitalcommons.library.uab.edu/etd-collection/6783>

This content has been accepted for inclusion by an authorized administrator of the UAB Digital Commons, and is provided as a free open access item. All inquiries regarding this item or the UAB Digital Commons should be directed to the [UAB Libraries Office of Scholarly Communication](#).

DESIGN, ANALYSIS AND DEVELOPMENT OF OPTIMIZED
THERMOPLASTIC PULTRUDED PROFILES

by

LEIGH A. HUDSON

UDAY K. VAIDYA, COMMITTEE CHAIR
DERRICK R. DEAN
SELVUM PILLAY
ALAN M. SHIH

A THESIS

Submitted to the graduate faculty of The University of Alabama at Birmingham,
in partial fulfillment of the requirements for the degree of
Master of Science

BIRMINGHAM, ALABAMA

2009

PROCESSING AND OPTIMIZATION OF A THERMOPLASTIC PULTRUSION PROCESS

LEIGH A. HUDSON

MATERIALS SCIENCE AND ENGINEERING

ABSTRACT

Thermoplastic resins have distinct advantages over thermoset resins, though they are more difficult to process due to their high melt viscosity. The present research focuses on the development and optimization of a pultrusion method for E-glass/polypropylene commingled tows. A thermoset pultrusion design was modified for the purposes of this research. Adaptations included a pre-heater to lower the temperature difference between the material and the ambient air before entering the heating die, a tow guidance system to aid in fiber alignment, and a die assembly specifically designed for the material consolidation requirements of thermoplastic resins. A parametric study was performed to determine the independent effects of die temperature, line speed and tow number on the material's properties. Mechanical testing was performed to determine the optimum material processing window. Both flexural and interlaminar shear (ILSS) testing indicated that greater tow numbers resulted in higher flexural and short-beam shear strengths. A heating die temperature of 430°C yielded the highest flexural strength (235.7 MPa) and short-beam shear strength (16.1 MPa). A pulling speed of 254 mm/min resulted in material with the highest flexural strength (228.5 MPa). The void volume percentage measured using optical microscopy was calculated for samples prepared at each temperature point and tow number. The microscopy results corroborated the results of the mechanical testing. The material processed at 430°C exhibited the lowest void volume percentage as well as the highest flexure and ILSS testing results.

Finally, finite element analysis was performed on an aluminum constant cross-section component to assess the feasibility of fabricating an equivalent part using thermoplastic pultrusion. Uniaxial continuous fibers exhibited 72.8% more deflection than the aluminum component under identical loading conditions. Other layup sequences and angle orientations were analyzed to attain balance of the bending and torsional loads. The optimum layup sequence was $[0_7/30/-30]_s$, which resulted in 15.75% more deflection than the aluminum component. The out-of-plane deflection can be further decreased by incorporating geometric stiffening elements into the component design.

DEDICATION

This thesis is dedicated to my husband Paul, whose love, patience, support and encouragement have been invaluable to me during this time. To my parents, John and Sherry Nolen, and to my brother, Dustin, for teaching me that through persistence and hard work, I can reach any goal.

ACKNOWLEDGEMENTS

I would like to express my gratitude to all those who made this thesis possible. I wish to thank Dr. Uday K. Vaidya for his guidance, both as a teacher and as an advisor. I would also like to thank Dr. Selvum Pillay for his direction and advice, which were indispensable, and to Drs. Derrick R. Dean and Alan M. Shih for lending their time and expertise to make this project a success.

I owe a debt of gratitude to Dr. Haibin Ning who gave selflessly of his time and was instrumental in helping me conduct the FEA portion of this thesis. In addition, I wish to thank the past and present members of the Engineering and Composites Lab who offered their assistance and support throughout this project, as well as Dr. Gregg Janowski and Jacob Putman for their technical assistance regarding die design. Andy Grabany, Balaji Thattai parthasarathy and Richard Phillips deserve a special commendation for their invaluable help during the design and testing phases.

Thank you to Peter Pfaff at Glasforms, who provided the pultrusion equipment, and to Don Hendry at Pinson Valley Heat Treating for his heat treating services.

Lastly, I would like to thank my husband, my parents, my brother and the remainder of my family for their love and their unwavering support throughout my educational career. They have been a source of strength for me when I needed it the most.

TABLE OF CONTENTS

	<i>Page</i>
ABSTRACT	i
DEDICATION	iii
ACKNOWLEDGEMENTS	iv
LIST OF TABLES	vii
LIST OF FIGURES	ix
INTRODUCTION	1
OBJECTIVES	4
LITERATURE REVIEW	5
Polymer Matrix Composites Processing	5
Pultrusion Processing	7
Thermoplastic Pultrusion	8
Focus of the Present Work	22
MODIFICATION OF THERMOSET PULTRUSION APPARATUS	23
Addition of Pre-heater with Integrated Guidance System	26
Addition of Heating and Cooling Die Assembly	29
MATERIALS AND EXPERIMENTAL METHODS	34
Material Form	34
Processing Method	35
Variation of Temperature	36
Variation of Tow Number	38
Mechanical Properties of Pultruded Components	38
Flexural Properties	39
Interlaminar Shear Properties	40
RESULTS AND DISCUSSION	42
Parametric Study	42
Variation of Temperature	42
Variation of Tow Number	43

Variation of Pulling Speed.....	44
Mechanical Properties of Pultruded Bars	45
Flexural Properties	45
Interlaminar Shear Properties	51
Microscopic Analysis.....	58
FINITE ELEMENT ANALYSIS OF A PULTRUDED THERMOPLASTIC COMPONENT.....	62
CONCLUSIONS.....	75
FUTURE WORK.....	79
LIST OF REFERENCES	80
APPENDIX.....	84
A THERMAL ANALYSIS DATA	84
B INTERLAMINAR SHEAR STRENGTH TEST DATA.....	86
C VOID VOLUME FRACTION DATA.....	92

LIST OF TABLES

<i>Table</i>	<i>Page</i>
1. Comparison of thermoset and thermoplastic resins	7
2. Effect of tow number on the void volume	60
3. Effect of temperature on the void volume	61
4. Properties of Aluminum 6061 used for FEA analysis of a TPX component.....	64
5. Properties of carbon fiber impregnated with PEEK resin.....	66
6. Deflection of aluminum and C/PEEK unidirectional fiber components under different loading conditions	68
7. Deflection values of various layup sequences of C/PEEK under different loading conditions.....	70
B-1. Dimensions of 95 tow sample for ILSS testing	87
B-2. Dimensions of 100 tow sample for ILSS testing	87
B-3. Dimensions of 420°C sample for ILSS testing.....	88
B-4. Dimensions of 430°C sample for ILSS testing.....	88
B-5. Dimensions of 440°C sample for ILSS testing.....	88
B-6. Dimensions of 450°C sample for ILSS testing.....	89
B-7. Dimensions of 381 mm/min sample for ILSS testing.....	89
B-8. Dimensions of 508 mm/min sample for ILSS testing.....	89
B-9. Dimensions of 635 mm/min sample for ILSS testing.....	90
B-10. Statistical analysis for ILSS testing of temperature samples	90
B-11. Statistical analysis for ILSS testing of tow samples	90

B-12.	Statistical analysis for ILSS testing of line speed samples	91
C-1.	Point count data for 95 tow material processed at 227°C.....	93
C-2.	Point count data for 100 tow material processed at 227°C.....	94
C-3.	Point count data for 105 tow material processed at 227°C.....	95
C-4.	Point count data for material processed at 215°C.....	96
C-5.	Point count data for material processed at 221°C.....	97
C-6.	Point count data for material processed at 227°C.....	98

LIST OF FIGURES

<i>Figure</i>	<i>Page</i>
1. Thermoset pultrusion apparatus	8
2. Thermoplastic pultrusion apparatus	9
3. Flow curves for Newtonian and non-Newtonian fluids	12
4. Thermoset pultrusion apparatus set up to process pre-impregnated tape before modifications.....	24
5. Thermoset pultrusion die	24
6. E-glass/PP [28] material feed set up	25
7. Current material set up to better guide and increase tension on tows A) tow arrangement around PVC tubing to increase tension B) guidance plate	25
8. System prior to the modification.....	26
9. Threading schematic of pre-heater showing tows routed around heaters (shown in gray) a) side view b) top view.....	28
10. Schematic of the guidance plates located in the pre-heater a) entrance plate b) center plate and c) exit plate	28
11. Heater locations within pre-heater	29
12. a) Lower section of heating die showing tapered and constant cross-section cavity b) heating die assembly	32
13. a) Lower section of cooling die showing constant cross-section cavity b) cooling die assembly	32
14. Die assembly and attachment.....	33
15. Twintex® rovings provided by Saint-Grobain Vetrotex [28].....	35

16.	Results from previous work showing the effect of die temperature on the pulling force [28]	37
17.	Results from previous work showing the effect of die temperature on line speed [28].....	37
18.	Flexure test of pultruded sample a) before loading b) after loading.....	40
19.	ILSS set up of pultruded sample a) before loading b) after loading	41
20.	Effect of temperature on line speed	43
21.	Surface quality of material pultruded with a) 95 tows b) 100 tows c) 105 tows indicating the increase in surface quality that occurs as the tow number increases.....	44
22.	Surface quality of material pultruded at a) 254 mm/min b) 508 mm/min c) 635 mm/min indicating the decrease in surface quality that occurs with increasing line speed	45
23.	Flexure sample after testing	45
24.	Close-up image of compression failure on flexure sample.....	46
25.	Effect of temperature on flexural strength	49
26.	Effect of tow number on flexural strength.....	49
27.	Effect of line speed on flexural strength.....	51
28.	Effect of temperature on shear force.....	52
29.	Short-beam strengths of material pultruded at 215°C, 221°C, 227°C and 232°C	53
30.	Common failure mode (interlaminar shear) that occurred during ILSS testing of glass/PP pultruded composites	54
31.	Effect of tow number on shear force.....	55
32.	Short-beam shear strengths of material pultruded with 95, 100 and 105 tows.....	56
33.	Effect of line speed on shear force.....	57
34.	Short-beam shear strengths of material pultruded at 254 mm/min, 318 mm/min, 508 mm/min and 635 mm/min.....	58

35.	Locations of photographs obtained for point count	59
36.	Microstructure of material pultruded at 221°C with a fifty-six point grid overlay.....	60
37.	General steps to perform FEA	62
38.	Cross-section of part geometry showing variable thickness.....	63
39.	Position of layers with respect to the composite mid-plane	65
40.	Forces and constraints applied to component TPX. Bolt holes circled in red were constrained for zero deflection a) side view of TPX component illustrating the 3558.6 N force in the negative y-direction b) side view of TPX component with 3558.6 N applied axially c) top view of component with 1334.5 N applied transversely	67
41.	Deflection from 3558.6 N load in the axial direction on a) aluminum component; values range from 0 mm (blue) to 0.1194 mm (red) b) C/PEEK continuous, uniaxial component; values range from 0 mm (blue) to 0.0635 mm (red)	68
42.	a) Von Mises stress distribution on upper portion of component from 1334.5 N applied transversely b) close-up view of maximum stress area; values range from 0 Pa (blue) – 9.03×10^8 Pa (red).....	69
43.	a) Von Mises stress distribution on side of component from 3558.6 N applied axially and in the negative y-direction and 1334.5 N applied transversely b) close-up view of maximum stress area; values range from 0 Pa (blue) – 1.32×10^9 Pa (red).....	70
44.	Deflections resulting from the combined loading scenario on a) $[0_7/45/-45]_s$ layup orientation; 20.96 mm deflection b) $[0_7/30/-30]_s$ layup orientation; 18.73 mm deflection	71
45.	a) Von Mises stress resulting from combined loading scenario for $[0_7/30/-30]_s$ b) close-up of maximum stress area, 1.36×10^9 Pa	72
46.	a) Von Mises stress resulting from combined loading scenario for $[0_7/45/-45]_s$ b) close-up of maximum stress area, 1.20×10^9 Pa	72
47.	a) Von Mises stress resulting from combined loading scenario for $[0_7/60/-60]_s$ b) close-up of maximum stress area, 1.23×10^9 Pa	73
A-1.	DSC results for Twintex® E-glass/PP commingled tows identifying the melting temperature of the matrix, which is observed to be 157.74°C.....	85

INTRODUCTION

Composite materials are two or more materials that, when combined, offer enhanced properties over those achievable with the constituent materials. Composite materials offer a wide variety of combinations that may be tailored for specific performance requirements. The constituent materials are selected based on the specific properties required for the application such as enhanced strength, increased toughness or corrosion resistance, as well as processing ease and economic feasibility.

Some common types of composite materials include metal matrix composites (MMCs), ceramic matrix composites (CMCs) and polymer matrix composites (PMCs) [1]. This research focuses on PMCs produced by a thermoplastic pultrusion process. PMCs are particularly suited for replacing metal parts, since they are lightweight and possess high specific strength-to-weight ratio. Composite materials are becoming more prevalent in mainstream applications within the construction, marine, and transportation industries due largely to the recent advances in processing capabilities combined with the greater availability of affordable high performance materials [2].

Each constituent of the composite contributes specific attributes to its final properties. Fibers generally provide high mechanical properties; however, they must be embedded within a matrix to be of practical use [1]. The matrix (e.g. thermosets and thermoplastics) holds the fibers in place, transfers the load between fibers and protects the fibers from abrasion and environmental attack. Interlaminar shear, compression and in-

plane shear are matrix dominated properties, while tensile properties are fiber dominated properties.

Two types of fibers are considered in this work – glass fibers and carbon fibers. Glass fibers are commercially popular because they provide relatively high strength for a low cost. They are non-flammable, electrically non-conductive and resistant to corrosion. Their primary disadvantages are low tensile modulus, sensitivity to abrasion (which can decrease their tensile strength) and low fatigue resistance [3].

Carbon fibers are used in applications which require higher tensile strength than provided by glass fibers. They are dimensionally stable during temperature changes due to their low coefficient of thermal expansion (CTE). They also offer much higher fatigue strength than glass fibers. On the other hand, the relatively high cost of carbon fibers prohibits their widespread use in commonplace applications. They exhibit low impact resistance. They are electrically conductive which could be detrimental to electrical equipment [3].

Composite materials differ from commonly used materials such as metals because their material properties are anisotropic, meaning that they are dependent on the fiber orientation. Composites are designed to provide strength in specific directions by orienting each lamina in those directions. Continuous, unidirectional fiber composites provide high strength when loads are parallel to the fiber direction. Finite element analysis (FEA) is often used to determine how a particular design will perform under specific loading scenarios.

Applications such as bridge decks, aircraft wings and waterfront protection sheet piles require dominant structural properties in the tensile direction. Pultruded composites

are well suited to create profiled sections with fibers aligned in the tensile loading direction. This research focuses on the design and optimization of a thermoplastic pultrusion process and the analysis of a thermoplastic pultruded composite component. An existing thermoset pultrusion apparatus is modified to process thermoplastic composite materials.

The work is organized as follows. First, a comprehensive literature review provides an in-depth discussion of polymer composite processing with a focus on the pultrusion method. The modification made to the existing pultrusion apparatus at the UAB Materials Applications Research Center is discussed. Parametric studies for thermoplastic pultrusion are then explained, and the mechanical testing results are discussed. A representative thermoplastic pultruded structural component is analyzed under different loading scenarios using FEA. Finally, conclusions and recommendations for future work are provided.

OBJECTIVES

The objectives of this research are to:

1. Adapt an existing thermoset pultrusion line to process thermoplastic composite pre-impregnated tapes and tows.
2. Investigate the effects of temperature, line speed and number of tows/tapes on the mechanical properties of the pultruded bars by performing flexure, interlaminar shear, tensile and low-velocity impact testing.
3. Conduct finite element analysis and optimization of a representative pultruded thermoplastic composite of a profiled cross-section.

LITERATURE REVIEW

Polymer Matrix Composites Processing

Natural polymers such as rubber, cotton and silk have been used for many centuries [4]. The past century brought about new technological advancements that led to the development of synthetic polymers which could be used in a far wider range of applications than their natural polymer predecessors. Synthetic polymers required the development of new processing methods before they could be successfully implemented.

Polymer composites are comprised of thermoset and thermoplastic resins. Thermoset processing involves mixing a resin and curing agent separately, infusing the mixture into the fibers and allowing the resin to cure at a specified temperature. Successful processing of thermosetting resins requires knowledge of the kinetics that occurs during polymerization and the result of these reactions on the viscosity and thermal properties [4]. Thermoplastic resins are formed by hot melt consolidation. During processing, the material is heated above the melting point of the resin, formed and allowed to cool until it solidifies completely. The rheology of thermoplastic polymers must be managed since their processing generally does not occur by exothermic reactions and cross-linking [4]. The appropriate processing method for either thermoset or thermoplastic polymer is dependent on the resin type, along with the viscosity and thermal properties.

Thermosetting resins offer certain advantages over thermoplastic resins. As a rule, thermosets offer thermal stability and chemical resistance, which makes them the

preferred option when an application calls for heat or corrosion resistance. Thermoset resins flow readily, facilitating fiber wet-out during processing. The cross-linked structures of thermoset materials effectively limit creep and stress relaxation that may occur in the polymer chains of thermoplastics [5].

There are several disadvantages of thermoset resins. Many thermoset resins release volatile organic compounds (VOCs) during processing, necessitating additional safety precautions. Special handling and storage requirements must be followed to prevent material degradation or excessive emissions. Growing environmental concerns have prompted research to develop fabrication processes using thermoplastic resins. Thermoset resins tend to be brittle and sensitive to impact loading.

Thermoplastic resins, on the other hand, generally do not require special storage or handling methods. Their scrap material can be recycled. Production is often more economical than thermoset production due to the shorter processing times required. On the whole, thermoplastics offer higher impact and fracture toughness than thermosets, as well as higher ultimate strain to failure [5-12]. A comparison of thermoset and thermoplastic properties is shown in Table 1.

Several processing methods are amenable to both resin types, differences in their curing kinetics and mechanisms notwithstanding. One method is pultrusion, a processing technique that produces continuous fiber-reinforced composite materials with a constant cross-section of infinite length [13]. The sections are cut to the desired lengths after processing has been completed. A wide range of industries including the transportation, automotive, aerospace, military, marine and agricultural industries utilize components that are particularly well-suited to the pultrusion process.

Table 1

Comparison of thermoset and thermoplastic resins

Resin Characteristic	Thermoset	Thermoplastic
Processing cost reduction potential	-	+
Simplicity of chemistry	-	+
Melt flow	+	-
Long prepreg shelf life	-	+
Low processing temperature	+	-
Low processing pressure	+	-
Low processing cycle time	-	+
Low cure shrinkage	-	+
Mechanical property shrinkage	+	-
Solvent resistance	+	-
Corrosion resistance	+	+
Toughness	-	+
Repairability	-	+
Recyclability	-	+
Low thermal expansion	+	-

Pultrusion Processing

Goldworthy pioneered the pultrusion method in the 1950's [2]. Glass fibers with polyester, vinyl ester or epoxy resin matrix were among the first materials to be processed using this technique. The early reinforcement fibers were continuous, uniaxial fibers. By the 1980's, mats made of knitted and multiaxial fabrics were being pultruded [2].

The pultrusion method has been used to process both types of resins, though it has been utilized more successfully for processing thermoset resins than thermoplastics. A thermoset pultrusion apparatus is designed to pull fibers through a guidance system and into a wet resin bath, where the fibers are impregnated. Once completely saturated, the fibers are pulled through a forming die to produce the desired part shape. The resin is

allowed to cure at a specific temperature before it is pulled out of the die. Once the material has sufficiently cooled, the parts are cut to the desired length. A schematic of this process is shown in Figure 1.

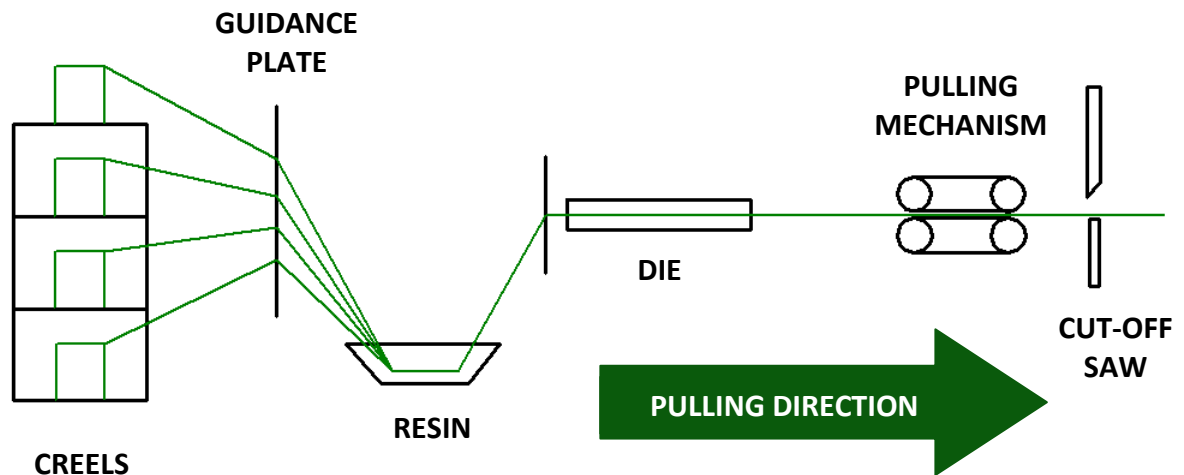


Figure 1. Thermoset pultrusion apparatus.

Thermoplastic Pultrusion

In spite of the advantages that thermoplastic resins offer over thermoset resins, the latter remains the materials of choice in the pultrusion industry. Differences in processing and material behavior require that modifications be made to the thermoset pultrusion apparatus [2]. A thermoplastic matrix is solid at room temperature and must be melted to mold it to the desired shape. More importantly, it must be cooled while in the mold for it to maintain its shape. The single die used in the thermoset process is unable to both heat and cool the material. It must therefore be replaced with a die assembly consisting of two dies – the first one for heating and the second one for cooling. A schematic of a thermoplastic pultrusion apparatus is shown in Figure 2.

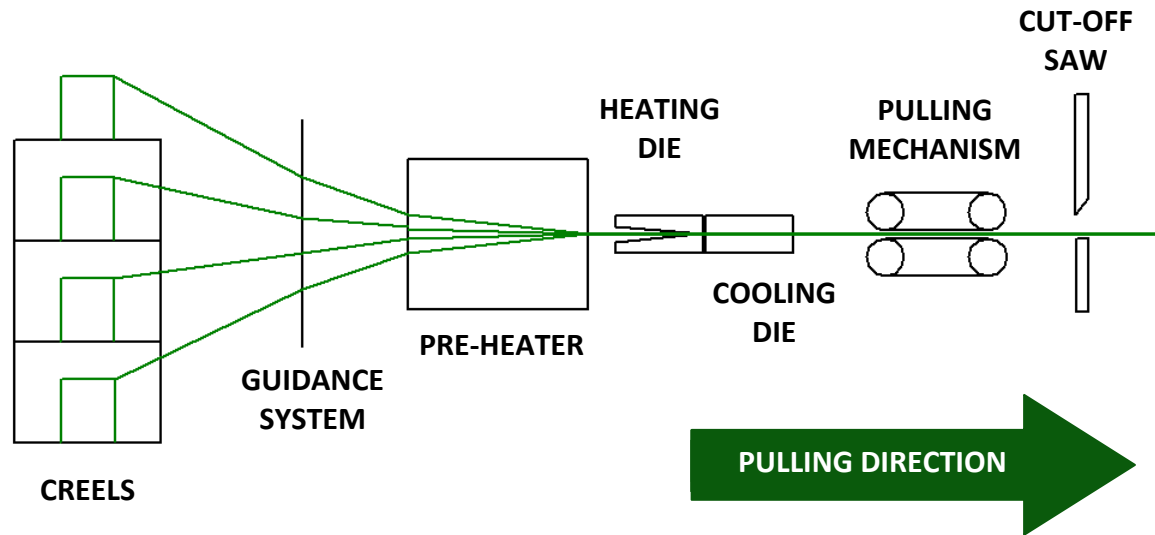


Figure 2. Thermoplastic pultrusion apparatus.

A number of difficulties associated with thermoplastic pultrusion have limited its use in industry. The design modifications in Figure 2 versus Figure 1 were necessary to facilitate thermoplastic processing. Thermoplastic resins possess much higher melt viscosities, usually two to three orders of magnitude higher than thermosetting resins [14]. This results in incomplete fiber saturation as the fibers are pulled through the resin bath. A different strategy must be employed for proper consolidation of the composite to occur. A material form that incorporates the matrix throughout the fibers is hence used in lieu of the resin bath [9]. This decreases the flow distance between the high viscosity matrix and reinforcing fibers, resulting in improved fiber wet out. The common material forms used in thermoplastic pultrusion include commingled fibers, powder impregnated fibers and hot melt impregnated fibers [8, 9, 15].

Material forms. Commingled tows consist of intermingled filaments of fiber and resin. The tows are processed by applying heat to melt the resin filaments and pressure to impregnate the reinforcement fibers. Resin fibers are often surface treated to create a sur-

face texture [16] or entwined throughout the tow to hold the fibers together since fibers are not consolidated in the preform [17].

Commingled tows can be made of any resin that can be spun into a fiber of the proper diameter [16]. Uneven distribution of the matrix strands can lead to resin-rich areas and dry regions in the final composite, which decrease mechanical properties [15]. This tendency can be controlled using reinforcement and matrix fibers of similar diameters [8, 16], though the cost of materials increases as the fiber diameters decrease [17].

Powder impregnated tows are produced by pulling the reinforcement fibers through a powdered resin so that the fiber's surface is covered in particles with diameters of 10 – 100 μm . The particles may be heated or a binder may be used to adhere the particles to the fiber surface [17]. Pins or rollers are commonly used to ensure that every fiber is evenly coated. The resin melts as it travels through the pultrusion die, impregnating the fibers via capillary action [8].

Hot melt pre-impregnated fibers are processed using a similar principal to pultrusion. The fiber tows are aligned and the filaments are spread to facilitate fiber wet out. The fiber tow enters a forming die that is attached to an extruder. Hot polymer melt is extruded into the die under high pressure and rapidly cooled as the material exits the die. The finished tape is collected on a take-up roll [5]. The structural fibers are completely impregnated during processing the tape, so the heated die needs only to perform the consolidation step. High processing speeds are attainable since the tape surface must only become molten to achieve complete consolidation.

Hot melt impregnated tapes are rigid, which can make them difficult to work with at times [18]. Commingled fibers are more drapable than tape. One the other hand,

commingled fibers are more difficult to process because fiber impregnation and fiber/matrix consolidation must occur within the heated pultrusion die. Greater control of processing parameters is essential to ensure that the resin fully melts, thereby allowing adequate flow, without reaching temperatures that could lead to thermal degradation of the polymer. As a result, flexible tow pregs require longer processing times on average, to allow the resin to melt and flow so that proper impregnation is achieved.

Polymer rheology. The rheological behavior of a thermoplastic must be understood to determine how the polymer flows as it moves through the pultrusion heating die. The viscosity of Newtonian fluids is affected by temperature and pressure [19]. Consequently, Newtonian fluids have linear flow curves. Thermoplastic resins, however, are non-Newtonian fluids, meaning that their viscosity is influenced by shear rate as well as temperature and pressure. Most thermoplastic materials are known to be pseudoplastic, or shear thinning polymers [20]. The apparent viscosity, (i.e. the ratio of the shear stress to the shear rate) of a shear thinning polymer decreases as the shear stress or shear rate increases. This is evident by the flow curve shown in Figure 3. Flow curves relate the shear stress and shear rate, and illustrate that the shear stress increases as the shear rate increases for pseudoplastic materials [21].

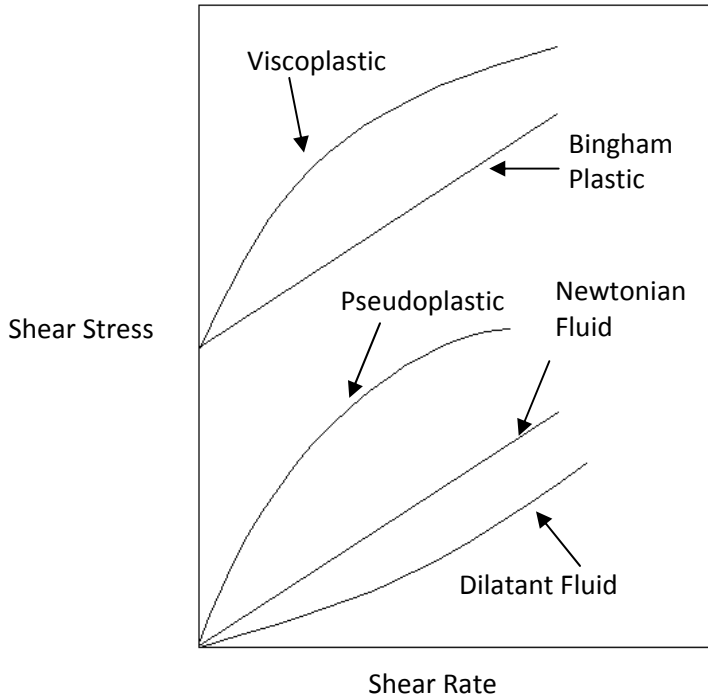


Figure 3. Flow curves for Newtonian and non-Newtonian fluids.

When a Newtonian fluid undergoes laminar flow, the shear stress is proportional to the product of the viscosity and the shear rate of the fluid. A non-Newtonian fluid requires a different model to predict the shear stress and apparent viscosity as they are functions of the applied shear rate [21]. The power-law is a popular model used to characterize the rheology of a non-Newtonian polymer. Two experimental constants are needed for each material to characterize its flow using the power-law. First, a measure of the fluid consistency is needed which can be related to the fluid viscosity. Second, a measure of the fluid's non-Newtonian behavior is also required. The shear stress and shear rate are related to one other with Equation 1.

$$\tau = m\dot{\gamma}^n \tag{1}$$

where τ is the shear stress, $\dot{\gamma}$ is the shear rate, m is a measure of the fluids consistency and n is a measure of the fluid's non-Newtonian behavior [21].

The apparent viscosity may be determined since $\eta = \frac{\tau}{\dot{\gamma}}$, using Equation 2:

$$\eta = m\dot{\gamma}^{n-1} \quad (2)$$

The power-law reduces to the Newtonian equation for viscosity when $n = 1$ [9, 20].

The rheological behavior of thermoplastic resins during pultrusion has been studied by several authors. Hepola [20] developed a unit cell model to predict resin flow among the continuous fibers as they are pulled through a tapered heating die. A one-dimensional model of the material system was developed which assumed that most of the resin flow occurs parallel to the fibers. The liquid resin was treated as a tapered annulus that surrounded each fiber [20]. This model can be used to describe both Newtonian and non-Newtonian fluids. The simplified equation of motion in the axial direction that Hepola [20] used is shown as Equation 3.

$$\frac{\partial p}{\partial z} = \eta \frac{1}{r} \frac{\partial}{\partial r} \left(r \frac{\partial v_z}{\partial r} \right) \quad (3)$$

where η is the viscosity, v_z is the velocity in the z -direction and r is the radius.

The boundary conditions for the resin were identified as

$$v_z = U \text{ at } r = \kappa R$$

$$\frac{\partial v_z}{\partial r} = 0 \text{ at } r = R$$

where R is the outer radius of the annulus, κR is the fiber radius and U is the pulling speed.

The act of pulling the reinforcement fibers through the die creates a drag flow in the resin. This drag flow was modeled as a plug flow, in which all elements of the ma-

terial move at the same velocity. The material flow rate must remain constant through the tapered section, allowing the flow rate to be calculated by the continuity equation, shown as Equation 4.

$$Q_{plug} = U\pi R(z)^2(1 - \kappa(z)^2) \quad (4)$$

The material exerts high pressure at the end of the taper, creating a pressure gradient that opposes the drag flow and produces a backflow of resin. The backflow may be calculated by integrating Equation 3, then integrating that result over the area to yield Equation 5.

$$Q_{backflow} = \int_0^{2\pi} \int_{\kappa R}^R v_z r \, dr \, d\theta \quad (5)$$

The total resin flow rate through the taper is the sum of the plug flow and the backflow. Equating the two flow equations describes the pressure gradient and the resin flow [20, 22].

The first step in processing thermoplastic matrix composites is impregnation. Impregnation occurs when the resin flows between the reinforcing fibers, completely wetting them. Lee et al. [23] developed sub-models for impregnation, consolidation and crystallinity of semi-crystalline thermoplastic composites. The impregnation sub-model predicts the degree of impregnation as a function of time. The model assumes the distance between adjacent fibers varied throughout the tow. The matrix surrounding the fibers coheres at these locations to form a resin bridge between the fibers. The matrix continues to join along the length of the fiber until it reaches another bridge location. Longitudinal flow is treated as laminar flow through an annulus. Radial flow is treated as flow through a porous medium. Experimental testing was performed with PEEK poly-

mer to determine the degree of impregnation in a T300 carbon fiber tow. The accuracy of the model is confirmed by the experimental results, which are comparable to the results predicted by the theoretical model.

The consolidation sub-model included models for intimate contact and autohesion. Intimate contact occurs when adjacent surfaces are brought into contact with one another and coalesce. The bonding that occurs at the interface is called autohesion. The intimate contact model predicts the degree of intimate contact, while the autohesion model predicts the degree of bonding and the time required to achieve both.

Sala et al. [9] mathematically modeled the longitudinal resin flow of powder impregnated tows using Newtonian and non-Newtonian approaches. The authors used the unit cell model approach previously discussed [20] to predict the effect of die length and pulling speed on pulling force and the effect of die length on the pressure distribution. The inlet and outlet dimensions of the die were held constant while the die length was varied. Their results showed that the pulling force decreased as the die length increased. This is due to a decrease in the taper angle, which decreases the back flow component while the drag flow component remains constant.

Miller et al. [8] developed impregnation and consolidation models for both powder impregnated tows and commingled tows. The model for powder impregnated tows relates how the void content changes as a function of time as the material travels through the heated die. The resin behavior is modeled on the assumption that the particles melt to form bridges between adjacent fibers. Each bridge that forms is assumed to be identical and forms between three fibers. The likelihood of formation depends on the specific particle size, the fiber diameter and the location of the fibers in relation to one another.

Resin flow along the fibers is induced by capillary forces as well as external pressure. The flow continues until each bridge meets an adjacent bridge, thus eliminating the void between them. The external pressure is opposed by the resin flow pressure, capillary pressure and compressive pressure as the fibers are squeezed in the transverse direction. The combined pressure field causes the longitudinal flow of the resin.

Miller [8] developed a different model to describe the flow behavior of commingled tows. The resin is in fiber form, so the majority of the flow takes place transversely. Flow through a fiber bed can be modeled as flow through a porous medium. Darcy's law, shown in Equation 6, is used to determine the flow velocity as related to the pressure gradient through the die.

$$U = \frac{dx}{dt} = \frac{SP}{\eta x} \quad (6)$$

where S is the permeability, η is the viscosity, P is the pressure and x is the distance. Equation 6 does not account for the resin's pressure dependence or non-Newtonian effects. Miller looked to previous work by Åström [24] where he modeled the power-law behavior during the impregnation process by using Equation 7.

$$\frac{dx}{dt} = \frac{k'}{Y} \left(\frac{P}{x}\right)^{\frac{1}{n}} \quad (7)$$

where k' and Y are constants and n is the power-law index.

The constant k' can be written in terms of pressure as shown in Equation 8.

$$k' = AP^{-m} \quad (8)$$

where A and m are constants. The velocity gradient can then be re-written as Equation 9.

$$\frac{dx}{dt} = \frac{A P^{\frac{1}{n}-m}}{Y x^{\frac{1}{n}}} \quad (9)$$

The model can determine the degree of consolidation as a function of pressure and time. It can also predict the optimum pressure and die contact time needed to obtain full consolidation of composites.

Darcy's law has been frequently used to describe the transverse flow of resin through a fiber bed. Kerbiriou et al. [18] developed an impregnation model for powder impregnated tows that models the fiber volume fraction and permeability as a function of time. The authors used Darcy's law to model the resin penetration rate through the fibers transversely as well as longitudinally. Kim et al. [15] constructed an impregnation model that incorporated a macroscopic resin flow sub-model. The process was modeled with a low shear rate, simplifying the resin behavior to that of a Newtonian fluid, allowing Darcy's law to predict the flow behavior.

Once impregnation is complete, material consolidation can begin. Consolidation is brought about via intimate contact and autohesion. The high viscosity of thermoplastic materials requires the application of heat and pressure to deform the material, in order to attain intimate contact. This contact brings about autohesion. The degree to which these phenomena occur is greatly influenced by temperature, pressure and time.

Effects of processing parameters. The pulling speed, temperature and tow number used have an effect on the outcome of the thermoplastic pultrusion. To determine an optimum processing window, a parametric study is needed to see how each parameter affects the mechanical properties of the pultruded parts. The optimization process is

complicated by the effect that changes in one parameter may have on the other two parameters.

Åström et al. [25] measured the pressure on glass reinforced polypropylene (GF/PP) as it was pulled through the heated die at different pulling speeds. All results show an abrupt pressure increase in the tapered portion of the die, which reaches a maximum at the point where the taper ends. The pressure decreases as the material moves through the constant cross-section of the die. The material must be held under pressure until it has fully consolidated. The pressure distributions showed that the tapered area of the die is critical to proper material consolidation.

The length of time that the material must be pressurized can be altered by manipulating the processing and design parameters. The time under pressure can be lengthened by decreasing the pulling force, but this can result in an unwanted pressure decrease. Decreasing the taper angle, which lengthens the taper, increases the time that the material is under pressure [25].

The magnitude of the pressure can be increased by broadening the thermal gradient within the tapered section of the die [25]. The resulting pressure increase would be attributable to the thermal expansion of the material. Decreasing the processing temperature will also increase pressure via an increase in the matrix viscosity. However, the temperature must be kept high enough to maintain flow of resin so as to enable fiber wet-out [25].

Åström et al. [25] measured the effect of the pulling speed on the force required to pull the material through the die. They determined that the pulling force increased as the pulling speed increased. The pulling force must be kept as low as possible to avoid fiber

breakage and to minimize die wear while still allowing for proper material consolidation. Proper consolidation requires a delicate balance of pulling speed, die temperature and confining pressure.

Pulling resistance is generated as the matrix flows in relation to the reinforcing fibers, and as a result of the shear forces that arise between the matrix and the die wall. The viscosity of the resin can be lowered by increasing the die temperature, allowing the resin to flow easily. Any temperature increases must be carefully monitored, as an increase in die temperature inversely affects the die pressure, causing it to decrease. The temperature must be maintained at a point sufficiently low enough to avoid thermal degradation of the material and to prevent a backflow of resin at the die entrance.

The material is formed and achieves maximum consolidation by the time it enters the constant cross-section portion of the heated die. As such, the length of the constant cross-section can be short. The pulling speed may also be reduced, as long as it does not reduce die pressure to the point where it inhibits consolidation. The length of the die taper can likewise be shortened, provided that the resulting decrease in time that the material is heated and pressurized does not cause problems with consolidation.

Fast pulling speeds produce a pressure increase as the material moves through the die [25]. The higher pressure is desirable from a material consolidation standpoint, though this benefit is negated if the higher speed leads to incomplete melting of the resin. Incomplete melting can also lead to higher pulling forces, brought about by an increase in pulling resistance due to a higher resin viscosity. The die temperature may also be increased to compensate for shorter melting times, provided it is not increased to the point that it causes thermal degradation or excessive resin backflow.

The amount of material needed to ensure adequate consolidation must be determined experimentally. Increasing the number of tows requires optimization of the heat input and polymer melting time. This can be accomplished with increased processing temperatures and/or slower pulling speeds. Using too many tows can result in overfilling the die, which can prevent the material from fully melting or increase the force needed to pull material through the die.

Weidmer [26] showed that void content of pultruded profiles increased at low pulling speeds when the heating die temperature is increased. He concluded that this condition resulted from a backflow of resin brought about by an increase in matrix viscosity at higher die temperatures.

Mechanical testing of pultruded composites. Mechanical properties of composite materials are influenced by the individual fiber and matrix properties, the surface characteristics, distribution, alignment and volume fraction of the fibers and the fiber/matrix interface. Mechanical testing of composite materials is further complicated by their anisotropic nature. This can lead to sample breakage at the grip area, unintentional failure modes and an improper balance between fiber and matrix dominated properties [27]. The nature of composite material necessitates specialized testing methods.

Defects resulting from the processing stage also adversely affect the mechanical testing results. Such defects include improper fiber alignment, kinked or broken fibers, uneven fiber/matrix dispersion throughout the composite, incomplete impregnation and voids. The testing process can inadvertently cause localized stresses in the composite at these points [27].

Weidmer [26] reported that shear properties decrease as pulling speed and/or die temperature are increased. Material pultruded at a rate of 10 cm/min exhibited a shear strength of approximately 45 MPa, which reduced to about 23% when pultruded at 70 cm/min. Flexural properties for material produced at a rate of 10 cm/min were about 460 MPa. This decreased to around 240 MPa when the pulling rate was increased to 70 cm/min. The flexural strength was not as significantly affected by variations in the heating die temperature. Material pultruded at both speeds did not have a significant drop until the heated die reached a threshold temperature.

Ma [11] studied the effect of fiber content on glass fiber reinforced Nylon 6 and the effect of pulling speed on Kevlar reinforced Nylon 6. He reported that the tensile strength of the glass fiber composites increased from 737.7 MPa for composites with a fiber content of about 45% by volume to about 855.0 MPa for those with a fiber content of about 58% by volume. The flexural strength increased as well from about 262.0 MPa to about 489.5 MPa for each respective fiber content. The flexural strength for Kevlar/Nylon 6 was shown to decrease from about 317.2 MPa at pulling speeds of 10 cm/min to about 296.5 MPa as pulling speeds were increased to 90 cm/min. Ma attributed the decrease in flexural strength to insufficient impregnation of the material brought on by a shorter residence time in the die at higher processing speeds.

Miller [8] studied the effect of line speed on the flexural strength of glass fiber polyamide 12 (GF/PA12) powder impregnated tows and glass fiber polypropylene (GF/PP) commingled tows. He reported that the GF/PA12 material had a flexural strength of about 680 MPa when pultruded at 1 m/min. The flexural strength decreased to about 570 MPa for pulling speeds of 10 m/min. The GF/PP composites had a flexural

strength of about 675 MPa at line speeds of 1 m/min which dropped to about 630 MPa when speeds were increased to 10 m/min.

Focus of the Present Work

The purpose of this research is to successfully fabricate thermoplastic composite materials using an existing thermoset pultrusion apparatus which has been specially modified to enable thermoplastic pultrusion. A parametric study has been performed to establish a processing window for the pultrusion of a fiber reinforced thermoplastic material system. Mechanical properties were determined for material processed under each of the conditions to determine which processing parameters yield the highest quality part. An existing high performance aluminum component was analyzed using FEA to determine the feasibility of producing the same part as a pultruded light-weight, fiber-reinforced thermoplastic composite.

MODIFICATION OF THERMOSET PULTRUSION APPARATUS

A thermoset pultrusion machine was modified to process thermoplastic composite materials as shown in Figure 4. The original design consisted of a sheet-metal tapered region that fed the tows into a heated thermoset die that measured 304.8 mm in length. Two 300 W cartridge heaters and a single 200 W cartridge heater provided heat to the die. A second die measuring 152.4 mm in length was situated immediately after the heated die. The two dies were bolted to each other to ensure close contact as shown in Figure 5. The material was pulled by a pneumatic clamping mechanism located 3.175 m from the die exit.

In the original design, the tows were draped over steel rods as they were pulled from the creel, shown in Figure 6. Figure 6 also shows the tendency of the tows to twist as they are pulled from the creel. If allowed to process in this manner, the fibers become crimped within the composite, decreasing the resulting mechanical properties of the pultruded profile.

Modifications were made to increase tension on the tows, which acts to minimize the inclination to twist. The material feed set up is shown in Figure 7. Each tow is routed around two steel rods covered in polyvinyl chloride (PVC) pipe in order to lower the surface friction in which the fibers must move across. The tows are routed in an S-shaped fashion, labeled as A in Figure 7. This arrangement provides the proper tension

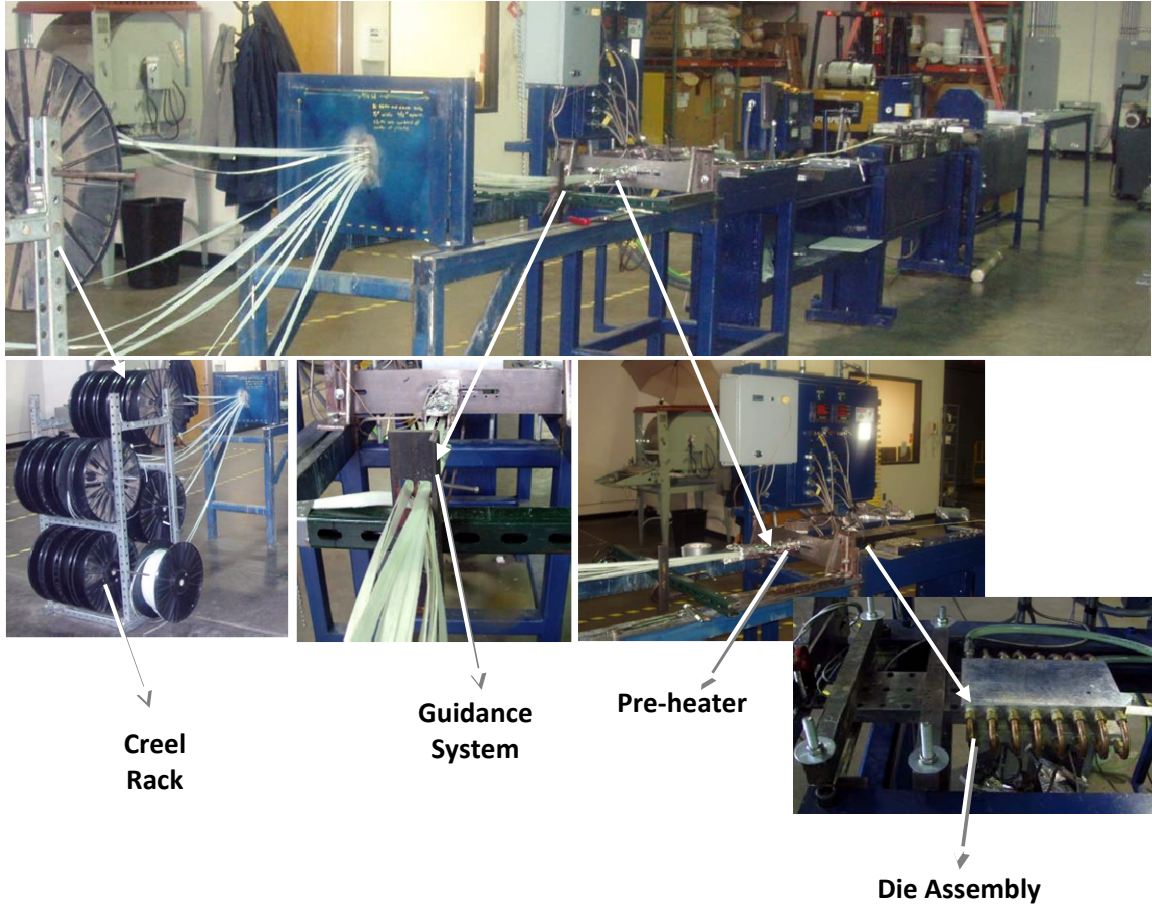


Figure 4. Thermoset pultrusion apparatus set up to process pre-impregnated tape before modifications.

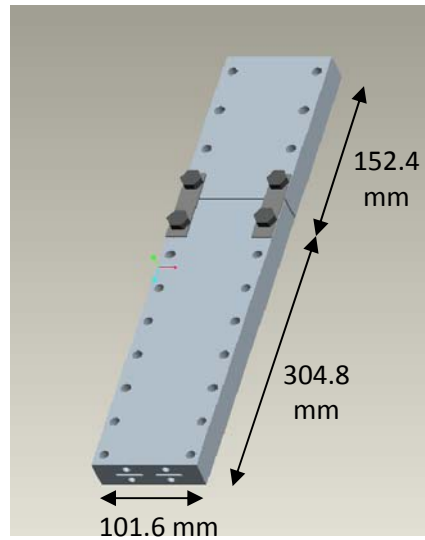


Figure 5. Thermoset pultrusion die



Figure 6. E-glass/PP [28] material feed set up.



Figure 7. Current material set up to better guide and increase tension on tows A) tow arrangement around PVC tubing to increase tension B) guidance plate.

to enable fiber alignment without creating excessive resistance in the fibers which would increase the pulling force needed during processing.

Addition of Pre-heater with Integrated Guidance System

A continuous, unidirectional fiber composite possesses highest mechanical properties when the fibers are aligned parallel to one another. The tows must be aligned as they are pulled from the creels and that alignment must be maintained as they move through the system. The existing guidance system and pre-heater in Figure 8 lacked the capability to properly align the fibers as they moved through and to maintain adequate alignment during processing.



Figure 8. System prior to the modification.

The pre-heater was also unable to generate sufficient heat to thoroughly and uniformly heat the material during its resident time. Previously pultruded components [28] showed sufficient melting and consolidation at the surface where the material directly contacted the heated die. Full consolidation, however, was not achieved in the central region, as it becomes increasingly difficult to heat the inner tows since the heat must

transfer to the center of the bundle. Experiments performed with higher die temperatures overcame the partial consolidation problem but led to discoloration of the exterior resin which is evidence of thermal degradation.

The new pre-heater is placed forward of the heating die to heat the resin almost to its melting temperature before it enters the die. This modification reduces the required melt time for the material while it is inside the heating die [15]. It is critical to maintain the temperature of the pre-heater slightly below the melt temperature of the polymer to avoid thermal degradation.

The material must exit the pre-heater and proceed directly into the heating die to prevent cooling. If the guidance plates are located after the pre-heater, the material would cool before it enters the die. A guidance system located prior to the pre-heater places the tows in a bundle, which requires a longer time for heat to transfer to the interior tows.

The new design integrates the guidance plates into the pre-heater. This adaptation accomplishes two objectives. First, it places the inner tows in closer proximity to the heaters, allowing them to be heated sufficiently. Secondly, it guides the tows into position to immediately enter the tapered die so that they retain the heat. This is depicted in the schematic shown in Figure 9.

The pre-heater is 1.0 m long. It incorporates three aluminum plates whose purpose is to guide the fibers through the pre-heater, stepping them down towards a central point so that they may be fed directly into the die. The first plate is located at the pre-heater entrance. It has thirty-five, 4.8 mm diameter holes that have been drilled at in a pattern that guides the fibers around the internal heaters. The second plate is positioned

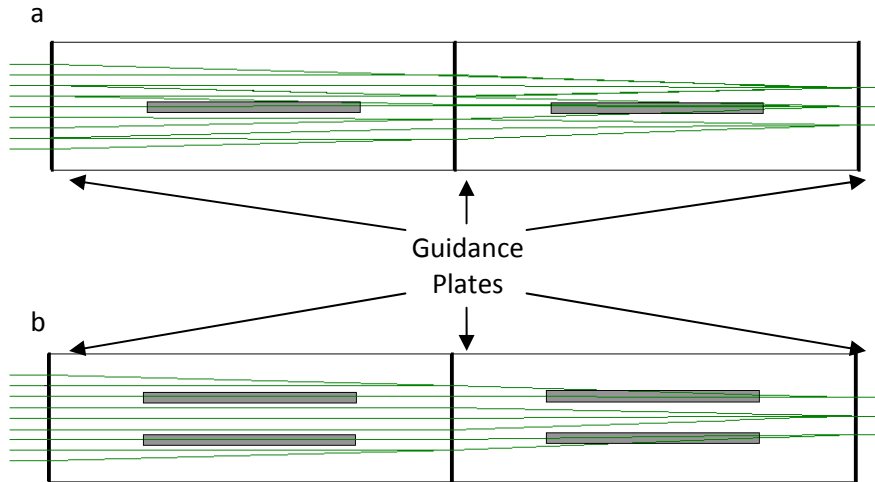


Figure 9. Threading schematic of pre-heater showing tows routed around heaters (shown in gray) a) side view b) top view.

at the midpoint of the pre-heater. It shares a similar drilled pattern as the first plate, but with only nineteen, 6.35 mm diameter holes. The last plate is situated at the exit point of the pre-heater. It has five 12.7 mm diameter holes drilled in the central region. The arrangement is depicted in Figure 10.

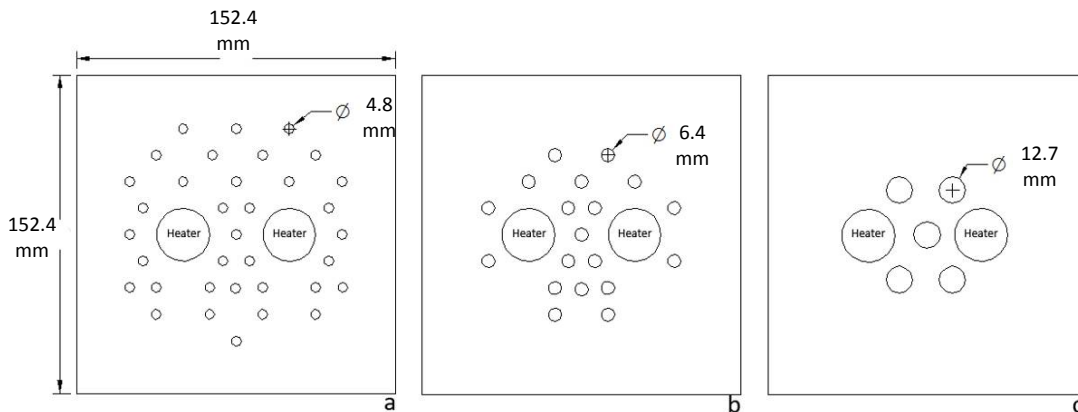


Figure 10. Schematic of the guidance plates located in the pre-heater (a) entrance plate (b) center plate and (c) exit plate.

Heat is supplied from a total of four 1000 W heaters inserted into metal sleeves. The heaters are placed in the center of the pre-heater so that the inner tows pass within close proximity, ensuring that they are adequately heated. The heater placement is shown in Figure 11. This layout successfully maintains proper fiber alignment, which will produce components with the highest possible mechanical properties.

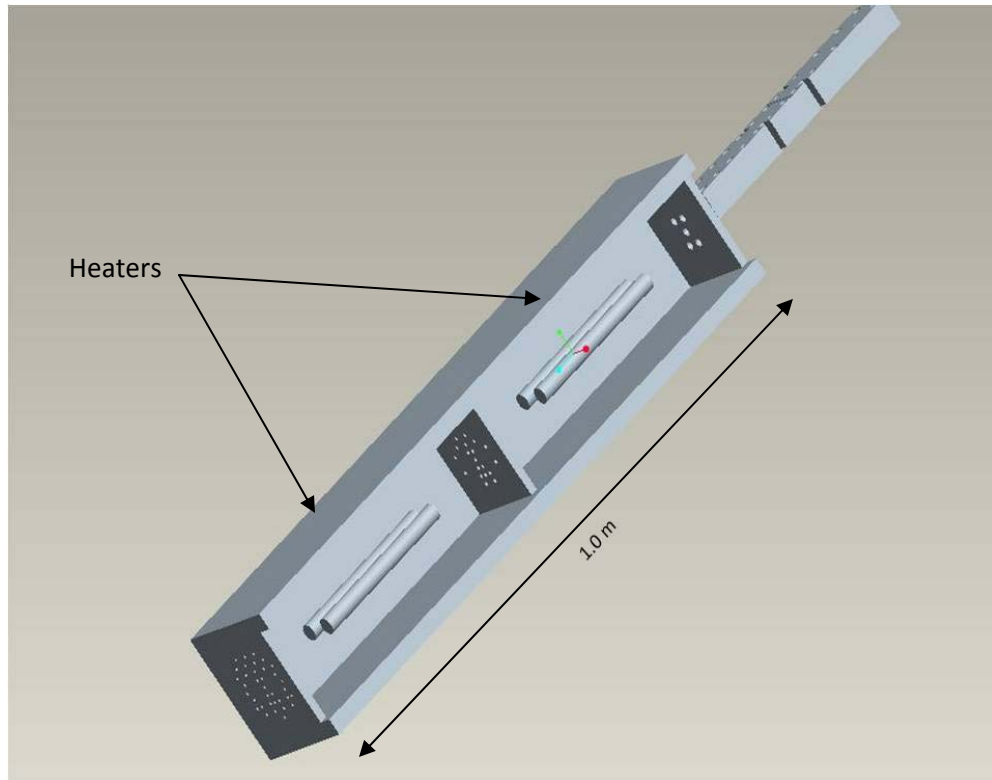


Figure 11. Heater locations within pre-heater.

Addition of Heating and Cooling Die Assembly

The single thermoset die is replaced by a thermoplastic die assembly. The new assembly consists of a combination heating/forming die to melt the resin and a cooling die to initiate crystallization. Thermoplastic heating dies are tapered over a majority of the die length [15, 29]. The taper decreases along the length of the die, creating a back-

flow of resin as the material is pulled through the die. As previously mentioned in the Literature Review section, the backflow causes a pressure increase that facilitates fiber impregnation and consolidation. By the time the material exits the tapered segment of the die, it should be fully impregnated and consolidated [15, 29].

Consolidation is maximized by ensuring that the composite is subjected to a fixed pressure for a minimum time period. Åström [25] demonstrated that the pressure rises as the composite travels through the tapered section of the die and decreases upon entering the constant cross section. His results indicate that higher pressure magnitude is obtainable by using longer die tapers (smaller angles). An additional benefit of the longer taper is that the composite remains under pressure for a greater period of time than with a shorter taper. This is a consequence of the increased flow that results from a longer melt time prior to consolidation. On the other hand, a shorter taper/larger angle consolidates the material faster, which allows heat to transfer more efficiently through the material [29]. According to Kerbiriou [18], a taper angle of 5° - 7° should yield the optimum material consolidation.

The die assembly was designed to process rectangular bars measuring 25.4 mm wide by 4.3 mm thick. The heating die, shown in Figure 12, is comprised of an upper and lower section bolted together using twelve $5/16$ inch (7.94 mm) bolts and two $3/8$ inch (9.53 mm) pins. Preliminary studies [28] showed that the material did not consolidate fully in the central region; therefore, the angle was chosen in an attempt to fully melt the resin. To allow the maximum time possible for the resin to melt, a taper angle of 5.5° was selected with this in mind. The rationale behind this choice was to apply pressure

gradually, allowing as much time as possible for the resin strands to melt prior to complete consolidation.

The cooling die is designed with a constant cross-section in place of the taper. The two halves are bolted together using eight 5/16 inch (7.94 mm) bolts and two 3/8 inch (9.53 mm) pins. A chiller is placed around the die to cool the material as it passes through. Coolant is circulated through the device to maintain the cooling temperature. The cooling die is illustrated in Figure 13.

A typical pultrusion die requires a surface hardness of 65 – 70 R_c [2]. This is usually obtained with surface coatings. There are a variety of choices, the most popular being a 30 – 40 R_c hardness steel that has been chrome plated, bringing the surface hardness to 70 R_c. The chrome layer is typically 0.0025 – 0.075 mm thick. Problems that can occur with chrome plated dies include the chrome surface stripping away from the die cavity. This can occur if the plating was applied incorrectly or if the material seizes in the die.

Dies may also be ion nitrided to increase their surface hardness. During ion nitriding, steel is bombarded with nitrogen in a vacuum. The nitrogen diffuses into the surface to form a thin layer that includes the original microstructure, nitride precipitates and a solid solution of nitrogen. The process is performed at temperatures below the austenitic temperature of steel, so quenching is not necessary, resulting in minimum part distortion. The surface hardness of the post-nitrided steel depends on the type of steel and alloying elements [30].

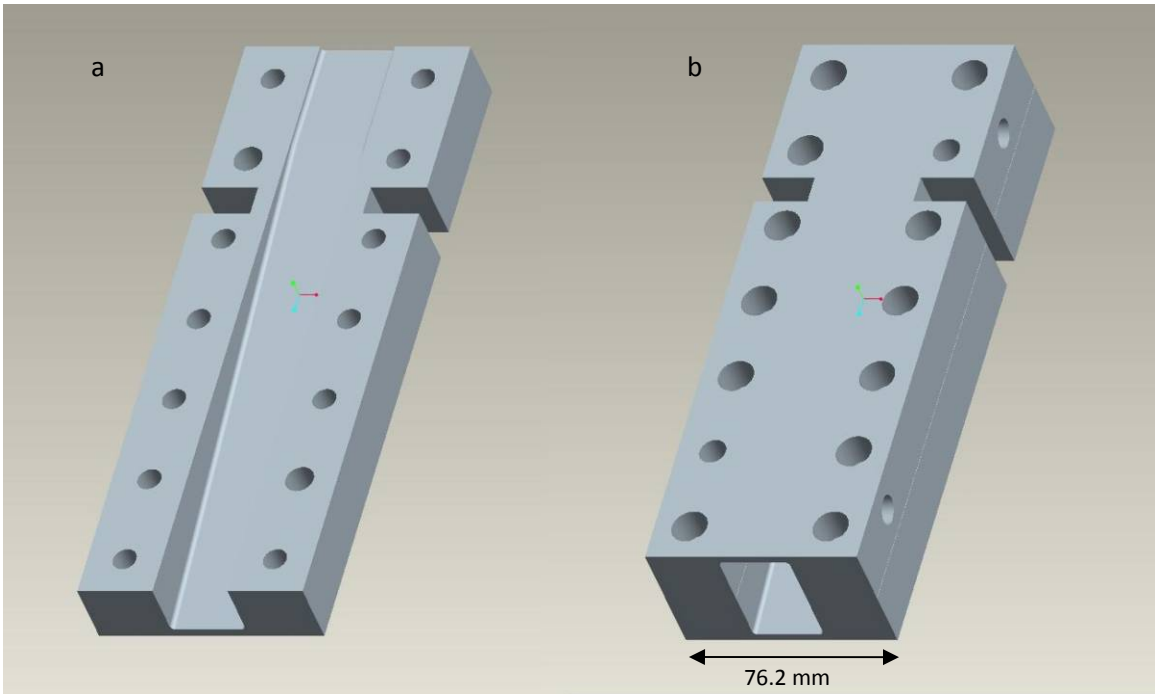


Figure 12. a) Lower section of heating die showing tapered and constant cross-section cavity b) heating die assembly.

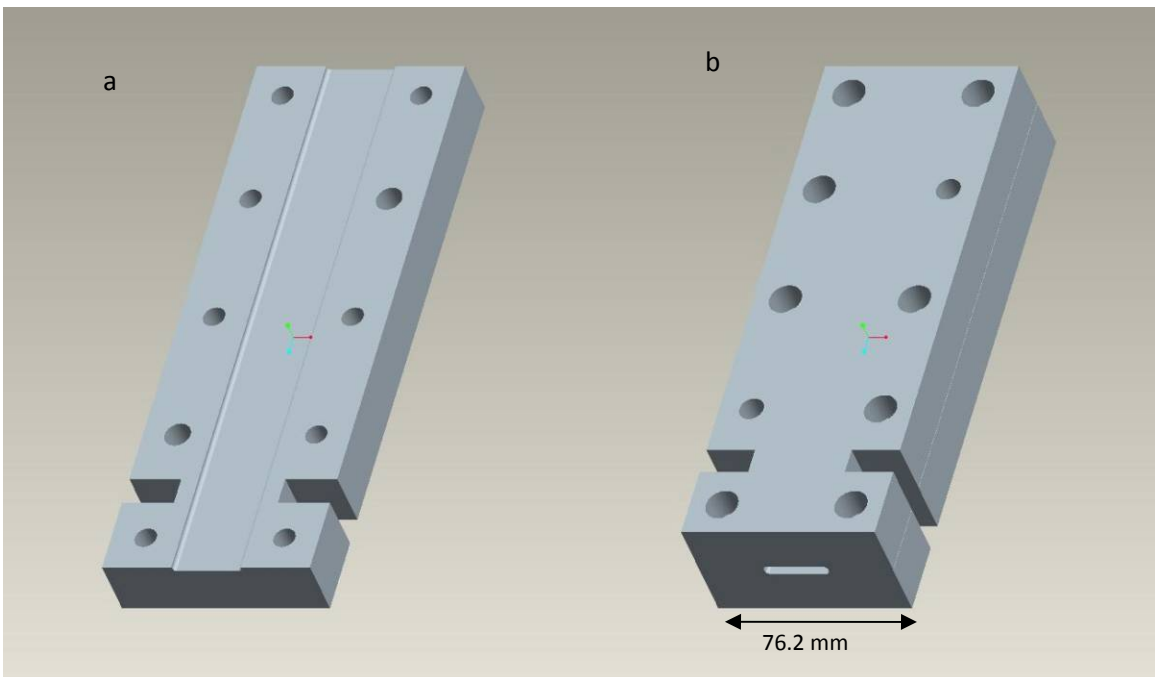


Figure 13. a) Lower section of cooling die showing constant cross-section cavity b) cooling die assembly.

Both dies were machined from 4140 steel plate and heat treated to a hardness of 52R_c. The heat treatment was necessary to decrease the ductility of the interior metal. Once the surface is hardened, the interior metal must be strong enough to prevent yielding which could result in surface cracks. A surface treatment was required to further increase the surface hardness, improve wear resistance and prevent corrosion. The surface was ion nitrided to a hardness of 64 R_c. A 3 micron post polish was performed in the cavity to reduce friction.

A high temperature graphite gasket is placed between the two dies. A clamping mechanism is utilized to secure them tightly together in order to prevent resin from flowing between the mated surfaces. The die assembly is attached to a fixed frame as shown in Figure 14 with a 0.5 inch (12.7 mm) diameter pin that allows the die to pivot.

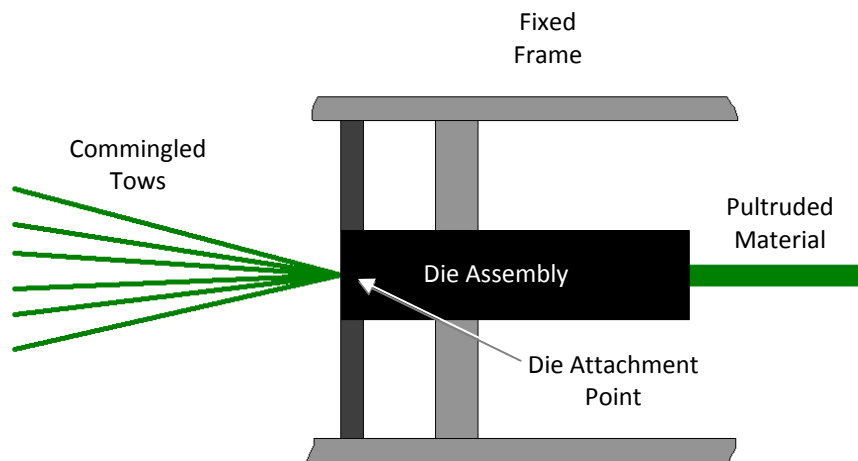


Figure 14. Die assembly and attachment.

MATERIALS AND EXPERIMENTAL METHODS

Material Form

Twintex® commingled rovings, procured from Saint-Gobain Vetrotex, were used. The material is shown in Figure 15. This product contains 75% by weight E-glass reinforcement and 25% PP resin homopolymer. The E-glass and PP filament diameters are 18 microns and 20 – 30 microns, respectively. This material form is well suited for pultrusion and filament winding.

The material was analyzed by performing Differential Scanning Calorimetry (DSC) to determine the melting temperature of the polypropylene matrix. The graphical results are shown in Appendix A as Figure A-1. The melting temperature was identified as 157.7°C. The company's processing recommendations suggest heating the rovings beyond the matrix melting temperature (specifically to between 180°C – 230°C), then applying pressure, followed by cooling while still under pressure.



Figure 15. Twintex® rovings provided by Saint-Grobain Vetrotex [28].

Processing Method

Material was routed from the creels through steel rods that were covered in PVC pipe. The fibers were then routed through a high-density polyethylene guidance plate, labeled as B in Figure 7. This plate aided in fiber alignment, while preventing fiber entanglement before the tows entered the pre-heater. The pre-heater was held at 149°C, slightly below the melting temperature of polypropylene. This temperature was chosen based on the material's appearance after exiting the pre-heater. At this temperature, there was no color change that would indicate thermal degradation to the polymer. The tows were guided through the pre-heater guidance plates and into the tapered portion of the heating die.

A single tow was first routed through the die. Multiple tows were added by tying them on to previous tows while ensuring each tow exited the die. The die was heated once the cavity of the die became full. Material was pulled to the clamping mechanism so that it could be pulled mechanically. At this point, the tows were marked and welded to previous tows at the die entrance to reduce the chance that one would become stuck at the end of the taper. This process was repeated until the desired number of tows had been fed through the die.

Variation of Temperature

Material was processed at heating die temperatures of 215°C, 221°C, 227°C and 232°C to determine the effect of the heating die temperature. The tow number and pulling speed were held constant at 254 mm/min and 105 tows, respectively. The pulling speed was measured manually to determine the effect of die temperature on the pulling speed.

The temperature variations were chosen based on the melting temperature obtained from DSC, the processing recommendations provided by the company and recent research by Kamble [28] using this material system. Previous results indicated a decrease in pulling force from about 1470 N to about 1415 N when the temperature was increased from 204°C to 210°C. The line speed increased from about 0.385 m/min to about 0.44 m/min at die temperatures of 204°C and 210°C, respectively. These results are shown in Figures 16 and 17.

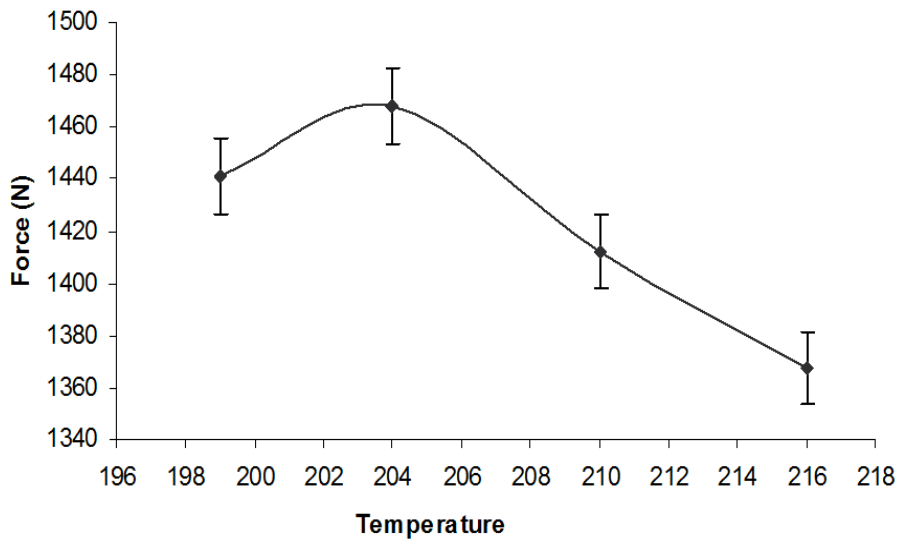


Figure 16. Results from previous work showing the effect of die temperature on the pulling force [28].

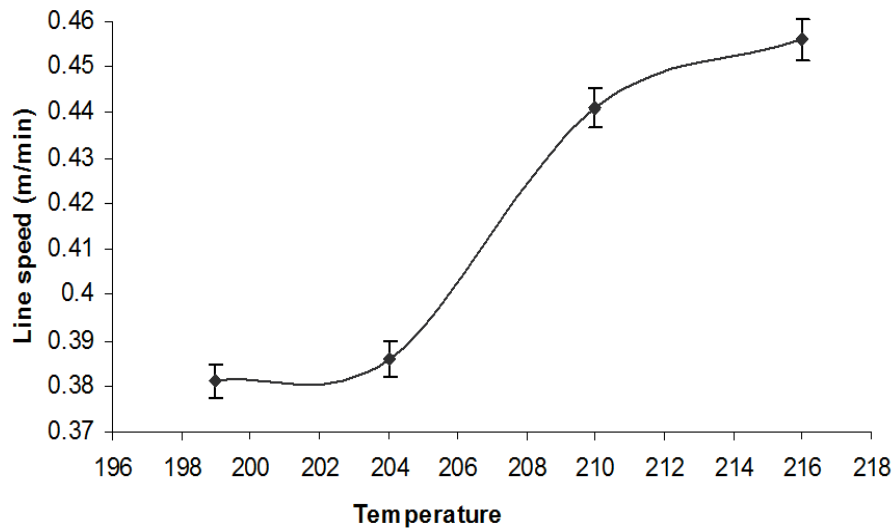


Figure 17. Results from previous work showing the effect of die temperature on line speed [28].

Variation of Tow Number

To achieve consolidation, the die must be adequately filled with material, without over filling it. Overfilling the die increases the pulling force required to pull the material through the die. As more material is pulled into the die, the pressure increases, which can eventually cause resin to flow out of the die entrance.

A calculation was performed to determine the theoretical number of tows that were required to completely fill the die cavity in a hexagonal close-packed pattern. The result indicated that 111 tows of the glass fiber volume fraction used in this study were needed to completely fill the die. The matrix material was assumed to fill the void regions completely. The calculated value assumes that each glass fiber is situated in a precise location with respect to adjacent fibers. The actual number of tows to be used during processing will be less than the theoretical value, since a perfect hexagonal close-packed arrangement of the fibers cannot be achieved.

Mechanical Properties of Pultruded Bars

Mechanical testing was performed to determine the optimum processing parameter combinations which would produce the highest mechanical properties. Mechanical properties are influenced by a variety of factors, including fiber and matrix properties, fiber alignment, processing details (e.g. fiber/matrix adhesion), and volume fraction of each constituent [27]. The properties resulting from each set of parameters will help determine the ideal specifications for producing parts of the highest quality.

Flexural Properties

Flexural testing is conducted to determine the flexural strength of a composite material. The specimen is placed in a three- or four-point bend to determine the flexural strength of the composite. The flexural strength is the stress at which the fiber fails in tension due to bending [5]. The span-to-depth ratio is large enough to promote increases in normal stress, while the interlaminar shear stress remains constant [31]. The properties are uniform through the composite thickness for uniaxial composites [27].

During the test, the sample witnesses maximum compression on the upper loading surface and maximum tension on the bottom surface. At the upper surface, the normal stress from compression decreases linearly to the mid-plane, where the tension begins to increase linearly until the maximum tension is reached on the bottom surface [27]. The maximum stress may be calculated using Equation 10.

$$\sigma_{max} = \frac{6M}{bh^2} \quad (10)$$

where M is the bending moment, b is the specimen width and h is the specimen thickness.

The shear stress can be calculated using Equation 11.

$$\tau_{max} = \frac{3F_s}{2bh} \quad (11)$$

where F_s is the shear force. The distribution is parabolic, beginning at zero at the upper and lower surfaces and reaching a maximum at the mid-plane.

Flexural testing was performed using a three point bending mode in accordance to ASTM D 790- 03, Procedure B using a span length of 64 mm. The testing was done using a Satec T-5000 Universal Testing Machine. The specimens measured 100 mm in length, 24.3 mm in width and 4.3 mm thick. The set up can be seen in Figure 18.

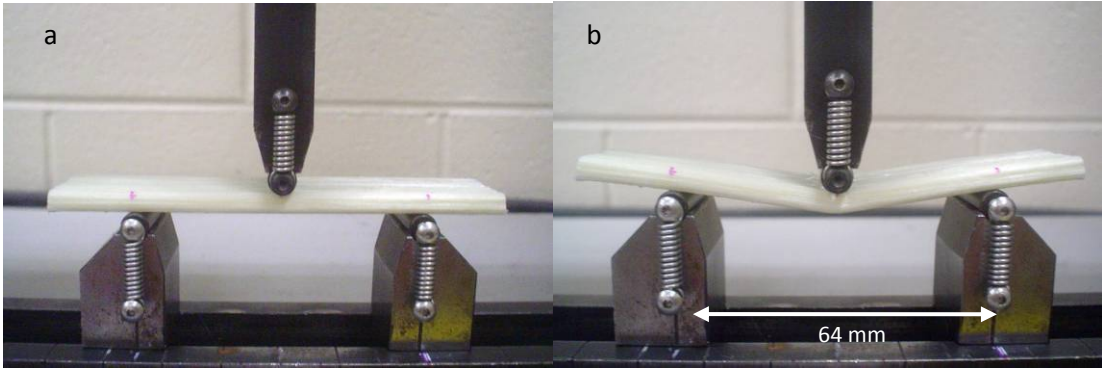


Figure 18. Flexure test of pultruded sample a) before loading b) after loading.

Interlaminar Shear Properties

Interlaminar shear is the shear that occurs between the fibers and the matrix when placed under a load. The maximum interlaminar shear stress may be calculated using Equation 12.

$$\tau_{max} = \frac{3P}{4bh} \quad (12)$$

where P is the load and b and h are the width and thickness of the specimen. Interlaminar shear strength (ILSS) can be determined experimentally by performing a short beam shear test. The span-to-depth ratio is low to create large interlaminar shear stresses at the mid-plane of the beam, where these stresses are the highest [31]. The short-beam strength is calculated using Equation 13.

$$F_{sbs} = 0.75 \cdot \left(\frac{P_m}{b \times h} \right) \quad (13)$$

where P_m is the maximum load occurring during the test, b is the specimen width and h is the specimen thickness.

ILSS is widely accepted as a major failure mode in composite material. For this reason, it is often used for quality control analysis. ILSS depends more on the matrix

tensile strength and the interfacial bonding between the fibers and the matrix. Values will generally decrease as defect content (voids, dry fibers, etc.) increases [5]. This trend makes it useful in determining the processing conditions that result in better fiber wet-out and produces fewer voids.

ILSS test results should not be used for design purposes. The shear stresses created during the test may not satisfy the requirements for the homogeneous beam theory from which the equation used to calculate the maximum stress is derived [5].

Interlaminar shear strength was determined according to ASTM D 2344 using a span length of 17.2 mm. The testing was performed on a Satec T-5000 Universal Testing Machine. The specimens measured 26 mm in length, 8.6 mm in width and 4.3 mm thick. The set up can be seen in Figure 19.

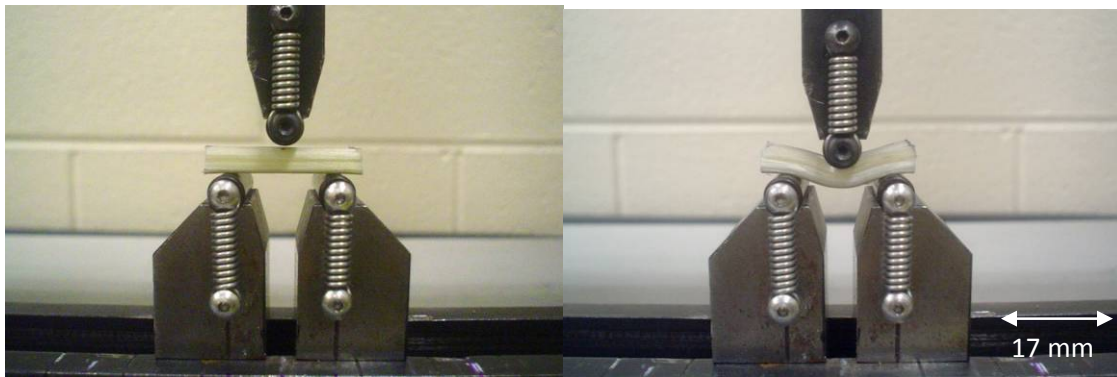


Figure 19. ILSS set up of pultruded sample a) before loading b) after loading.

RESULTS AND DISCUSSION

Parametric Study

Variation of Temperature

The results shown in Figure 20 indicate that the line speed increases from 625.6 mm/min to 628.6 mm/min between the temperatures of 204°C and 210°C. This is consistent with previous results [28] showing that the line speed increases significantly between these two temperatures. The line speed decreases drastically from 628.6 mm/min at 216°C to 622.6 mm/min at 221°C. This decrease in line speed is possibly brought on by a decrease in resin viscosity at 221°C. Increased flow would lower the resistance between the resin and the die as the material travels through the die. Lower resistance requires a lesser pulling force to process the material. Above a certain threshold viscosity, the resin backflows as the material is pulled through the taper. This was discussed in detail in the Literature Review. The backflow creates a pressure which can help to consolidate the material. However, excessive pressure can increase die wear.

As the temperature increases from 221°C to 227°C, the line speed also increases from 622.6 mm/min to 629.4 mm/min. The increased temperature decreases the melt viscosity of the resin, also reducing the backflow pressure and, consequently, the resistance between the resin and the die cavity. The lower melt viscosity allows the resin to flow and wet-out the fiber filaments properly. The increased flow of the resin at 227°C decreases the amount of die wear that might otherwise occur at lower

temperatures. The material pultruded at each temperature showed little variation in surface quality.

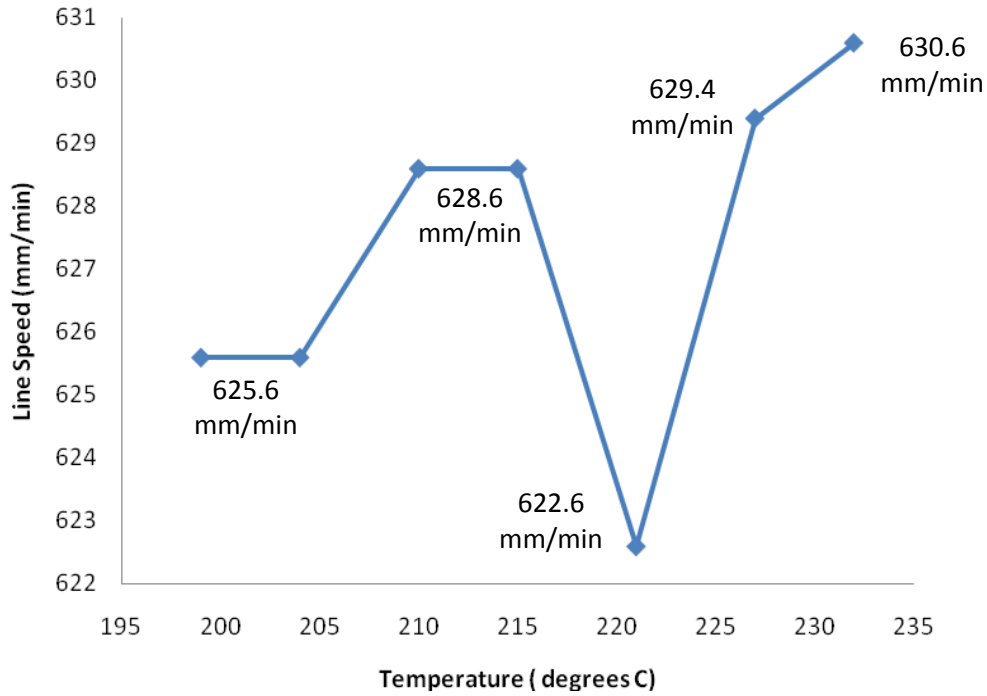


Figure 20. Effect of temperature on line speed.

Variation of Tow Number

Material pultruded using 95, 100 and 105 tows is shown in Figure 21. Longitudinal ridges are seen in areas of all material pulled, though they are deeper and most frequently in the material with 95 tows. This indicates that the material volume in the 95 tow composite was insufficient to fill the die. The ridges become shallower and less frequent in the material pultruded with 100 and 105 tows as can be seen in Figure 21. In-

creasing the material volume within the die cavity produced a composite with a smoother material surface.

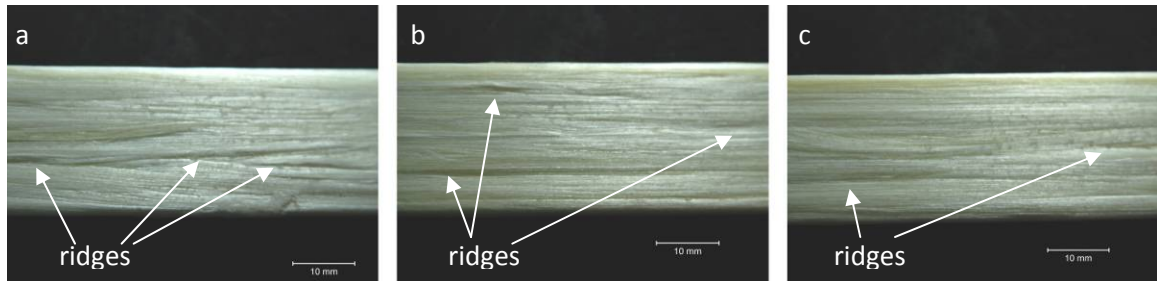


Figure 21. Surface quality of material pultruded with a) 95 tows b) 100 tows c) 105 tows indicating the increase in surface quality that occurs as the tow number increases.

Variation of Pulling Speed

The material pultruded at 254 mm/min exhibited the smoothest surface. Faster processing speeds tended to produce rougher surfaces by comparison. Shorter heating times are unable to heat the resin to achieve the same melt viscosity that longer heating times produce. Upon entering the cooling die, the part surface cools faster than the interior. Friction between the die wall and the material increases as the line speed increases. The resin viscosity increases as it cools and the resin in contact with the die begins to shear as the material moves through the die cavity. The surface quality of the material pultruded at 254 mm/min, 508 mm/min and 635 mm/min is shown in Figure 22. The surface becomes progressively rougher at processing speeds of 508 mm/min and 635 mm/min. The surface relief of the 381 mm/min sample is very similar to that of the 254 mm/min sample and is, therefore, not shown.

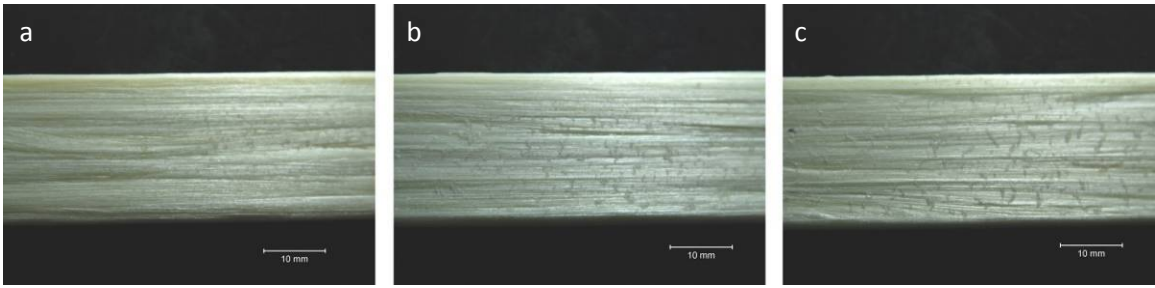


Figure 22. Surface quality of material pultruded at a) 254 mm/min b) 508 mm/min c) 635 mm/min indicating the decrease in surface quality that occurs with increasing line speed.

Mechanical Properties of Pultruded Bars

Flexural Properties

A representative specimen tested for flexure is shown in Figure 23. Each specimen failed in compression at the outer surface as shown in the figure. The back surfaces showed no evidence of damage.

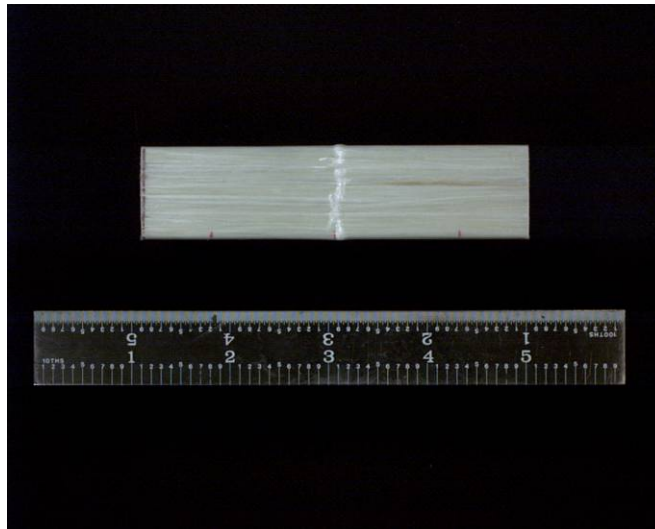


Figure 23. Flexure sample after testing.

Figure 24 shows a magnified image of the failure area. The typical failure mode of a uniaxial composite loaded in transverse compression is shearing between the fibers and matrix. This behavior often leads to debonding of the fiber/matrix interface or fiber damage. The figure shows fiber misalignment at the compression site, which is evidence that shearing occurred while the compression load was being applied. Transverse properties of a unidirectional composite are known to be matrix dominated. None of the samples experienced catastrophic failure during testing, a fact which can be attributed to the long polymer chains of thermoplastic materials. The strain capacity of the polymer provides the chains sufficient time to untangle, rather than break. The characteristic toughness of thermoplastics is due in large part to this tendency.



Figure 24. Close-up image of compression failure on flexure sample.

Effect of temperature on flexural properties. The material processed at 215°C yielded the lowest flexural properties (222.9 MPa) of the four temperatures (215°C, 221°C, 227°C and 232°C) tested. The melt viscosity of the resin at this temperature is not low enough to produce sufficient resin backflow in the die taper. Additionally, the higher melt viscosity does not allow resin to flow effectively through the fiber filaments.

The flexural results shown in Figure 25 show that the highest properties are obtained at a processing temperature of 221°C. The material pultruded at 221°C exhibited an ultimate flexural strength (UFS) of 235.7 MPa. Referring to the results in Figure 20, the line speed decreased from 628.6 mm/min to 622.6 mm/min as the die temperature was increased from 215°C to 221°C. As discussed with the results in Figure 20, lower melt viscosities produce backflow inside the taper that creates a pressure gradient inside the die. This pressure increase aids in material consolidation. The maximum flexural properties suggest that a die temperature of 221°C (for material processed at 254 mm/min) produces the best combination of melt viscosity and pressure for material consolidation.

The material pultruded at 227°C and 232°C had a UFS of 229.3 MPa and 231.9 MPa, respectively, an average of 1.6% lower than material processed at 221°C. Referring once again to Figure 20, these temperatures provided the highest pulling speeds (629.4 mm/min and 630.6 mm/min) of all of the temperatures studied. The resin viscosity at these temperatures is lower than the resin viscosity at 221°C, allowing the resin to flow easier. The loss of backflow pressure resulting from a lower viscosity may explain the slightly lower flexural strength for material pultruded at the two higher temperatures. For material pultruded at 227°C and 232°C the loss of flexural strength is offset to some

degree by the decreased die wear resulting from lower resistance as the material is pulled through the die.

Figure 25 also shows that the flexural modulus of the material processed at each temperature is identical up to 0.001 strain. Above this point, the modulus becomes lower for the material processed at 215°C and 221°C.

Effect of tow number on flexural properties. Flexural results for material pultruded using 95, 100 and 105 tows are shown in Figure 26. The flexural strength increased as the tow numbers increased. This was expected since the number of tows processed was below the theoretical value of 111 tows previously calculated. The material processed with 95 tows results in the lowest UFS of 151.1 MPa. Increasing the tow number to 100 tows increased the UFS to 179.2 MPa, 15.7% higher than the material pultruded with 95 tows. Adding five more tows, increased the UFS to 235.4 MPa, 23.9% higher than the material pultruded with 100 tows. The strength increase is attributed to an increase in material volume within the die, which increased reinforcement fiber content as well as the consolidation pressure. The modulus is lowest for the material processed with 95 tows. The modulus increased as the tow numbers were increased. The additional material also increased the processing pressure at the end of the die taper which increased the degree of consolidation.

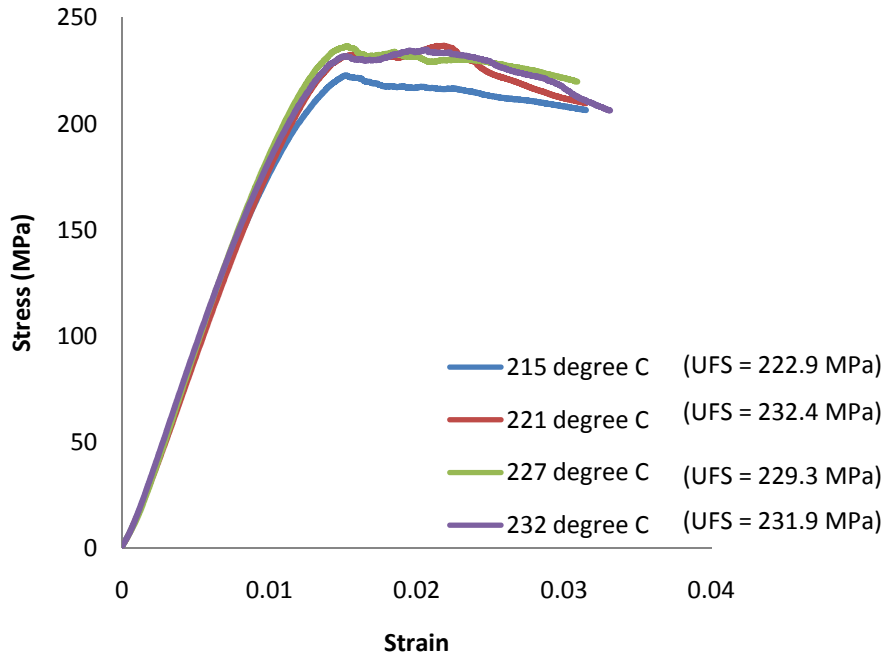


Figure 25. Effect of temperature on flexural strength.

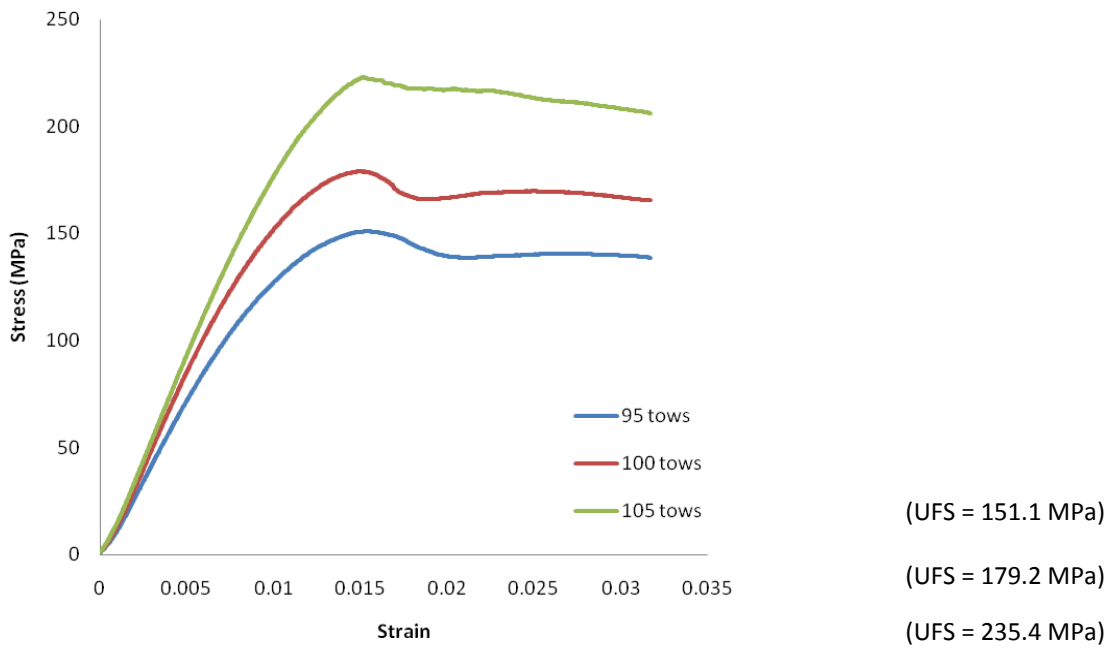


Figure 26. Effect of tow number on flexural strength.

Effect of line speed on flexural properties. Figure 27 illustrates that the highest UFS (228.5 MPa) occurred in the material pultruded at 254 mm/min versus the other line speeds of 381 mm/min, 508 mm/min and 635 mm/min. The polymer is exposed to heat for a longer time at this speed which resulted in the lowest melt viscosity and highest resin flow of the speeds studied. The second highest UFS (226.7 MPa) resulted from a line speed of 508 mm/min, which is 0.79% lower than the material pultruded at 254 mm/min. Although the resin's melting time is decreased significantly at this speed, the higher melt viscosity produced a larger resin backflow within the die taper. The pressure increased sufficiently enough to promote resin flow through the fiber network. The material pultruded at 635 mm/min exhibited a decrease in UFS to 183.5 MPa. This is 24.5% lower than the strength of the material pultruded at 254 mm/min. The strength decrease for the material pultruded at 635 mm/min suggests an inability to achieve melt viscosities to allow the resin to adequately flow at this speed. The material pultruded at 381 mm/min resulted in the lowest UFS of 180.3 MPa, 1.6% lower than the material pultruded at 635 mm/min. The melt viscosity of the resin at this speed is lower than it is at 508 mm/min. It may still, however, remain too high to flow easily through the fibers. This particular combination of melt viscosity and pulling speed may not be capable of producing adequate backflow pressure in the die taper in order to assist the resin flow.

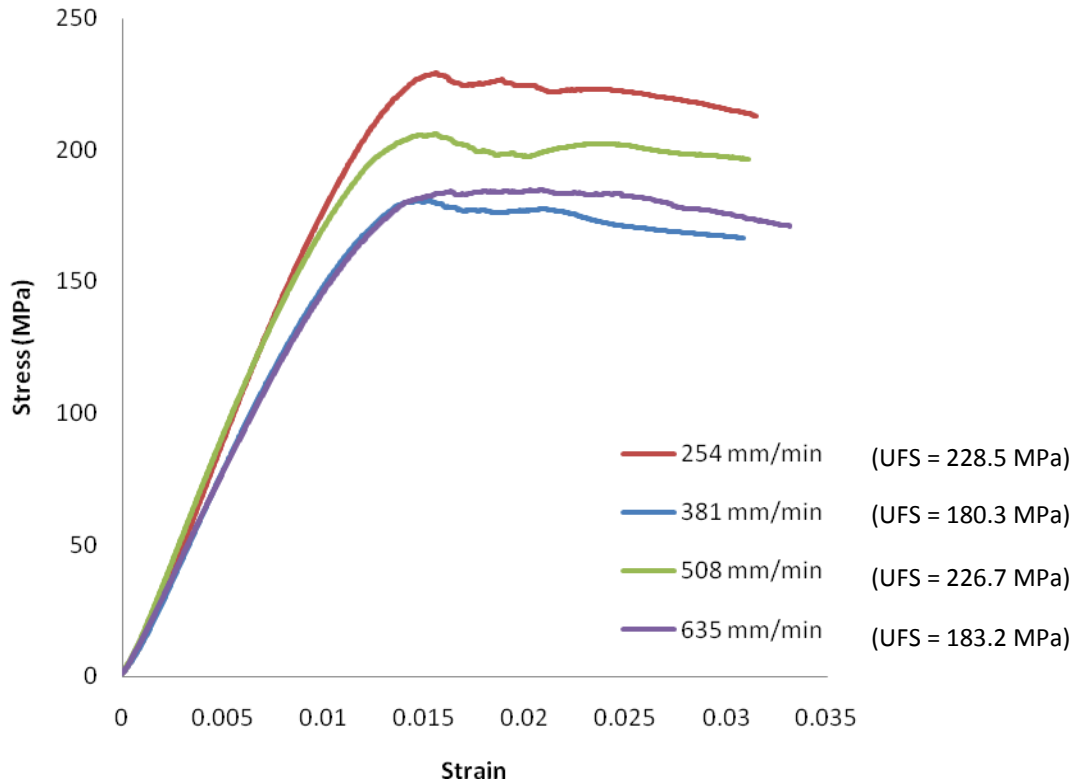


Figure 27. Effect of line speed on flexural strength.

Interlaminar Shear Properties

Effect of temperature on shear properties. Load/deflection curves for material processed during the temperature study are shown in Figure 28. The material pultruded at 221°C withstood 798.1 N, the highest load achieved by any of the processing temperatures studied. Material processed at 215 °C and 232 °C resulted in smaller loads of 784.0 N (1.8% smaller) and 771.66 N (3.4% smaller), respectively. Processing at 227°C resulted in the minimum load of 730.5 N, which was 9.3% lower than the highest load (798.1 N).

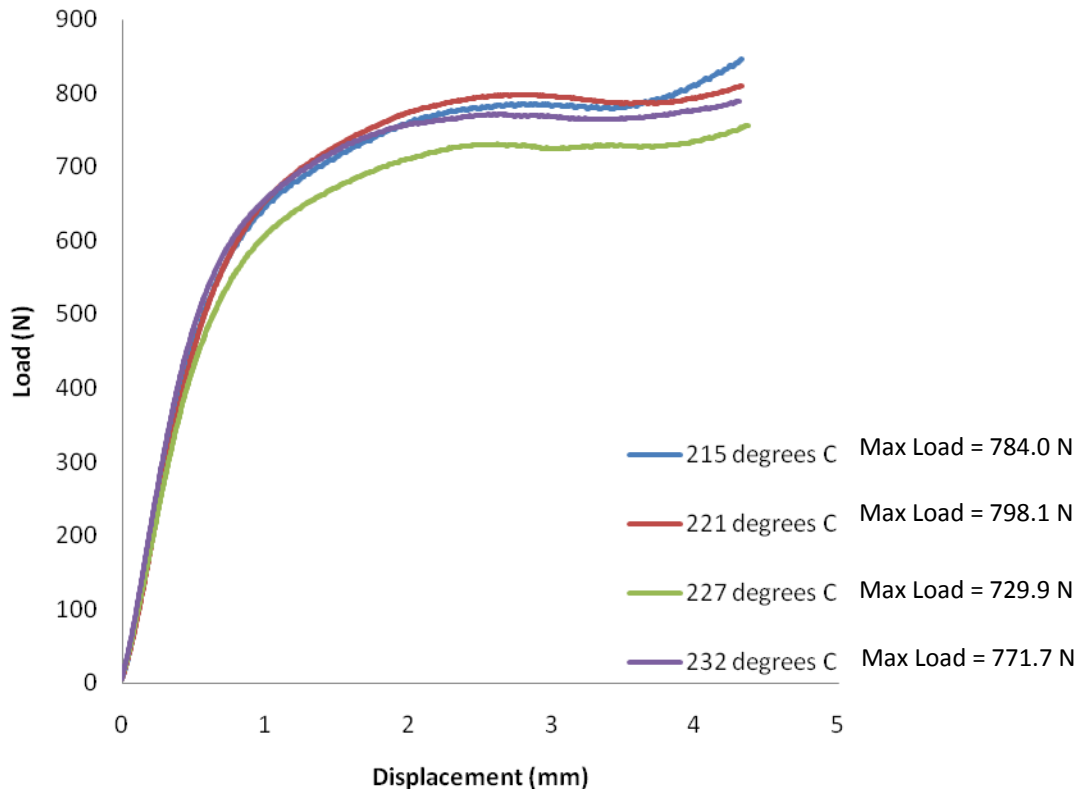


Figure 28. Effect of temperature on shear force.

The short-beam strengths calculated for the initial peak of each sample are shown in Figure 29. The material processed at 221°C resulted in a short-beam strength of 16.1 MPa. The material processed at 215°C and 232°C resulted in slightly lower short beam strengths of 15.7 MPa (2.5% lower) and 15.5 MPa (3.9% lower), respectively. The lowest short-beam strength was calculated for the material pultruded at 14.9 MPa, 8.1% lower than the material pultruded at 221°C.

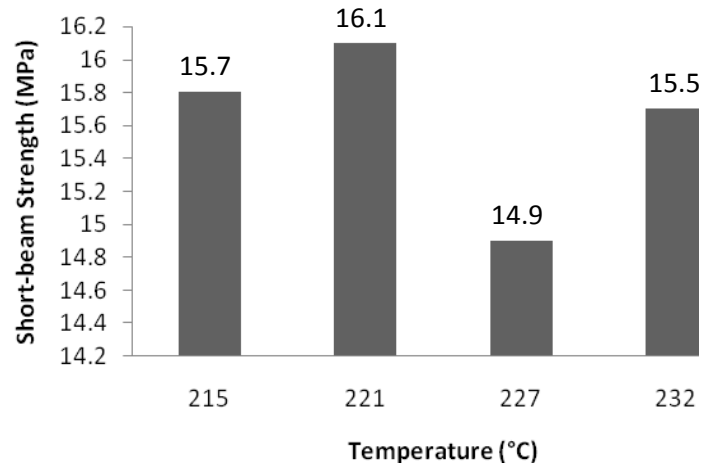


Figure 29. Short-beam strengths of material pultruded at 215°C, 221°C, 227°C and 232°C.

The typical failure mode resulting from a transverse compressive load is matrix shear failure. Matrix shear failure leads to interface debonding as well as fiber damage [31]. An example of a typical failure mode for a uniaxial pultruded composite is shown in Figure 30. The specimen shows cracks at the end brought about by interlaminar shear between the fibers and matrix. As previously mentioned, the shear stress in a beam reaches a maximum at the mid-plane, where the normal forces are zero. Figure 30 shows that the cracks initiated close to the mid-plane on both sides of the composite and propagated through the thickness. It is likely that the crack progressed along weaker areas that did not achieve maximum consolidation.

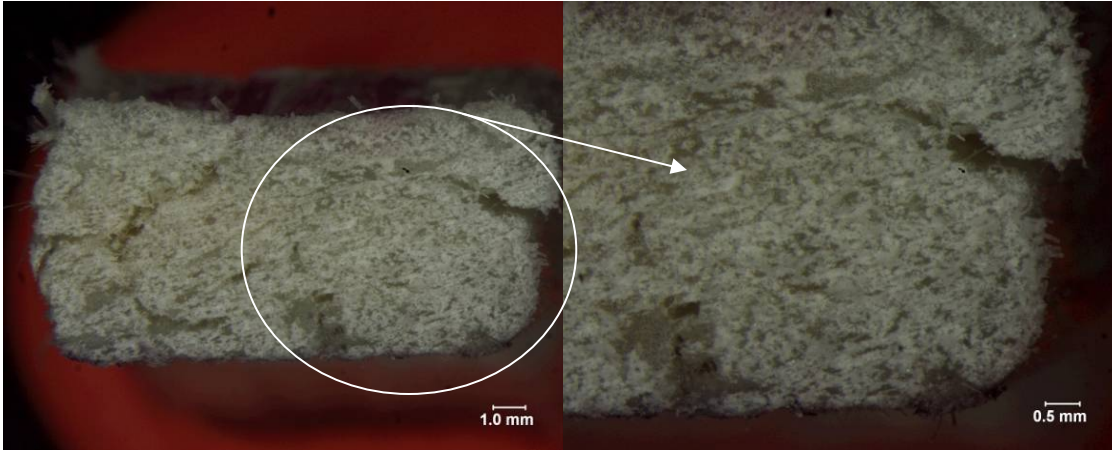


Figure 30. Common failure mode (interlaminar shear) that occurred during ILSS testing of glass/PP pultruded composites.

Effect of tow number on shear properties. The shear strength increased as tow numbers were increased. This was anticipated, since a higher material volume increases pressure within the die, thereby increasing material consolidation. Shear properties are highly influenced by the quality of the interface of the resin and the fibers. Voids and dry regions act as locations of stress concentration, allowing stress to build until the onset of shear failure.

The results are shown in Figure 31. There is no distinguishable peak for material pultruded with 95 and 100 tows. The load values at a displacement of 2.5 mm, (the location of the initial peak in the 105 tow sample) will, therefore, be compared for each tow number.

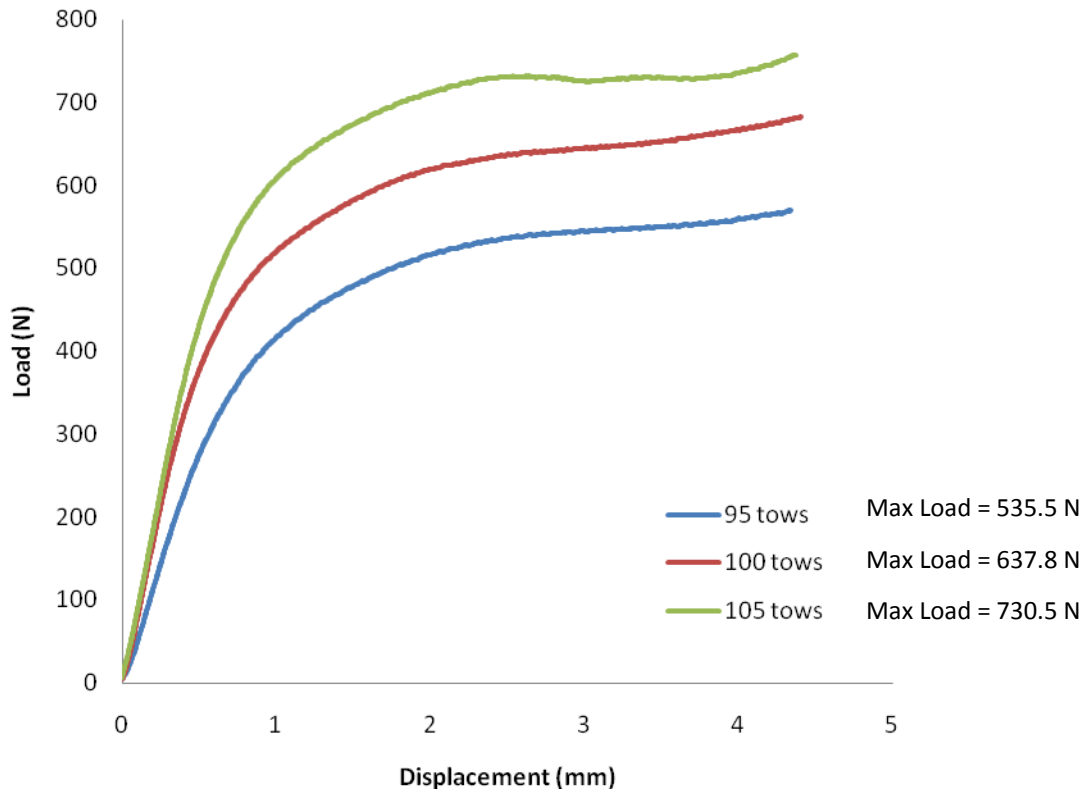


Figure 31. Effect of tow number on shear force.

The load occurring at 2.5 mm for the material pultruded with 95 tows is 535.5 N. The material pultruded with 100 tows is able to withstand a load of 637.8 N, 16.0% higher than the 95 tow sample. The highest load, 730.5 N, results from the material pultruded with 105 tows. This load is 12.7% higher than the material containing 100 tows and 26.7% higher than the material containing 95 tows.

The short-beam strengths are shown in Figure 32 for each sample at a displacement of 2.5 mm. The short-beam strength of the material pultruded at 95 tows is 11.0 MPa. The material containing 100 tows is 12.8 MPa, 16.4% higher than the material

containing 95 tows. Finally, the material pultruded with 105 tows resulted in a short-beam strength of 14.9 MPa, 35.5% higher than the material pultruded with 95 tows.

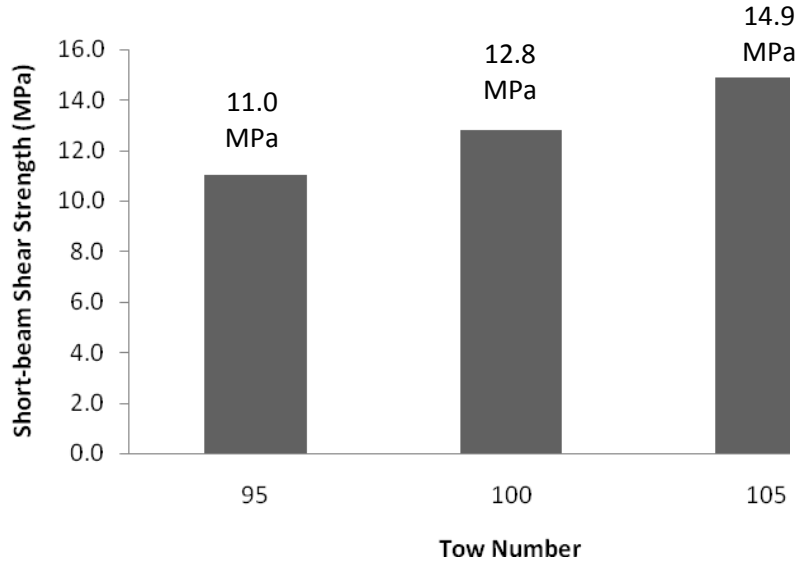


Figure 32. Short-beam shear strengths of material pultruded with 95, 100 and 105 tows.

Figure 31 also illustrates that the shear modulus increased as tow numbers increased. The increase in both strength and modulus is due to the increased pressure that results from a die containing a higher material volume.

Effect of line speed on shear properties. The test results in Figure 33 show that the material pultruded at 381 mm/min exhibited higher shear stress compared to the material pultruded at 254 mm/min, 508 mm/min and 635 mm/min, reaching a maximum load of 749.2 N at a deflection of 2.5 mm. The material processed at 254 mm/min performed 2.6% lower, reaching a load of 730.5 N at a deflection of 2.5 mm. A faster pulling speed allows less residence time in the heating die, resulting in higher resin viscosity and higher backflow in the die taper. This creates a higher pressure in the die when

compared to lower viscosity resin pulled at slower speeds. The material pulled at 508 mm/min and 635 mm/min exhibited the lowest loads, 697.7 N and 680.2 N, respectively, 7.4% and 10.1% lower than material processed at 381 mm/min.

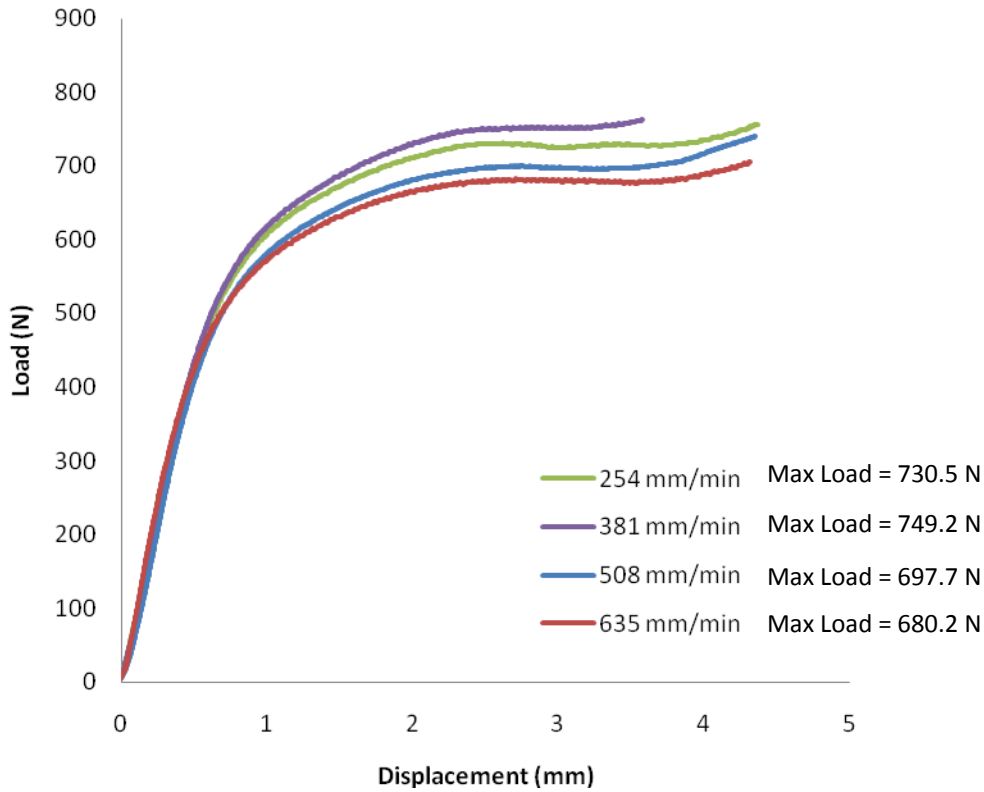


Figure 33. Effect of line speed on shear force.

A comparison of the calculated short-beam shear strengths are shown in Figure 34. The highest value, 15.5 MPa, resulted from the material pultruded at a line speed 318 mm/min. The second highest value, 14.9 MPa, resulted from a pulling speed of 254 mm/min, 4.0% lower than the material processed at 318 mm/min. The material produced at 508 mm/min had a short-beam shear strength of 697.7 mm/min, 6.2% higher than the

material pultruded at 318 mm/min. The lowest short-beam shear strength (680.2 MPa) occurred for the material pultruded at 635 mm/min. This value is 12.3% less than the short-beam shear strength of the material pultruded at 318 mm/min.

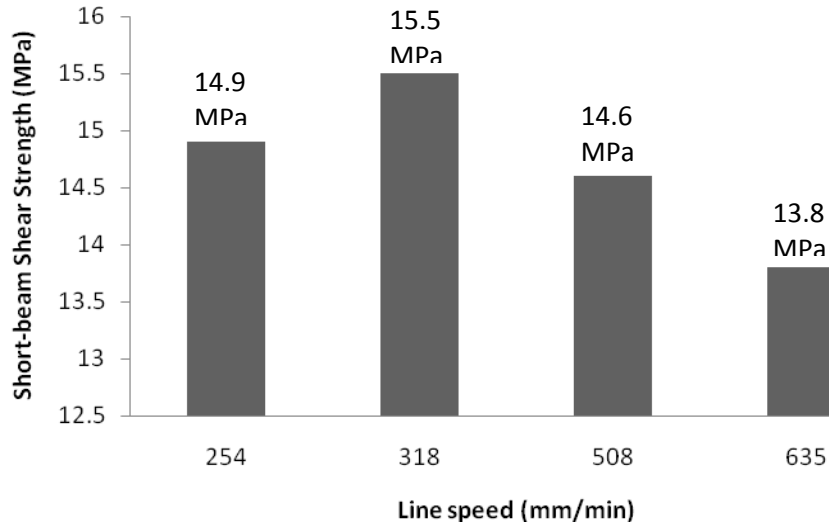


Figure 34. Short-beam shear strengths of material pultruded at 254 mm/min, 318 mm/min, 508 mm/min and 635 mm/min.

Microscopic Analysis

Material processed at each temperature and tow number was cross-sectioned, mounted, polished and viewed using an Axioplan optical microscope to determine the effect of each processing parameter on the microstructure. Twenty photographs were obtained at 100X magnification with the sample locations chosen over the entire material area to yield representative results of the entire composite cross-section. The picture locations are shown in Figure 35.

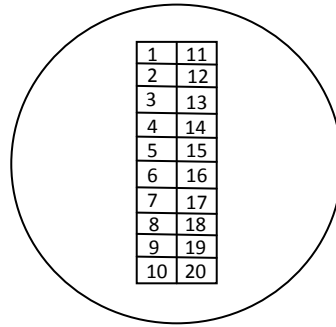


Figure 35. Locations of photographs obtained for point count.

A manual point count was performed in accordance to ASTM E562-95 to determine the void percentage in each composite. A fifty-six point grid was selected to perform the point count over twenty photographs to yield a relative accuracy of 20%. A photograph with the grid overlaid is shown in Figure 36. Each void that was located at the grid point was counted and each boundary that fell on the grid point was counted as a one-half void. If it was not possible to determine whether the point fell on a void or boundary, a value of one-half was recorded for that point to prevent bias from entering the results.

Data from the individual point counts are provided in Appendix C. The results for the number of tows are summarized in Table 2. The void count decreased as the number of tows increased. This was expected due to a greater volume of material filling the die. The variation from ninety-five tows to one-hundred tows resulted in a 14.8% decrease in the void volume. The void volume decreased further (23.0%) from 100 tows to 105 tows.

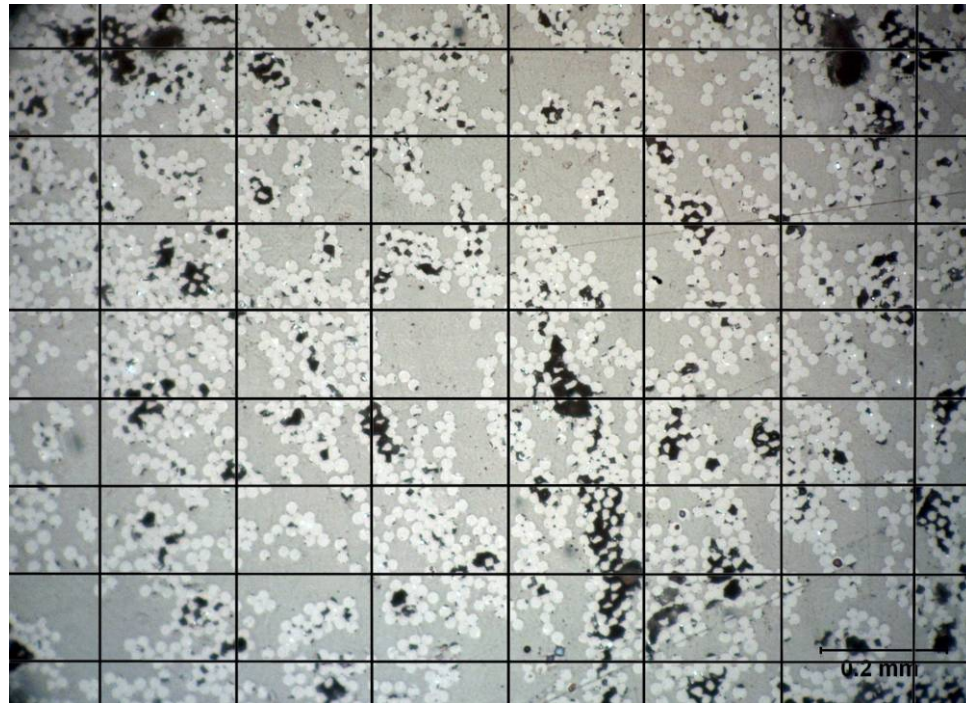


Figure 36. Microstructure of material pultruded at 221°C with a fifty-six point grid overlay.

Table 2

Effect of tow number on the void volume

Number of Tows	95	100	105
Mean, X (%)	32.95	28.71	23.35
Standard Deviation, S (%)	3.73	5.38	4.37
95% Confidence Interval (%)	1.75	2.52	2.04
Relative Accuracy (%)	5.3	8.8	8.8
Coefficient of Variation	0.025	0.042	0.042
Void Volume Percentage (%)	31.2 – 34.7	26.2– 31.2	21.3 – 25.4

The results from the temperature study are shown in Table 3. Processing at a temperature of 221°C resulted in the lowest void volume of 15.2 – 20.9%. This processing temperature appears to result in the most consolidated material which corre-

lates well with the mechanical testing results showing that this material had better properties in bending and interlaminar shear.

Increasing the temperature to 227°C and 232°C resulted in a 27.6% increase in the mean point count, with similar values in the actual percentage of void volume. These results are consistent with the data reported by Wiedmer [26]. The highest void volume resulted in the material processed at 215°C, which was 5.9% higher than the material processed at 227°C and 232°C.

Table 3

Effect of temperature on the void volume

Temperature (°C)	215	221	227	232
Mean, X (%)	24.82	18.07	23.35	23.35
Standard Deviation, S (%)	3.35	6.14	4.37	5.30
95% Confidence Interval (%)	1.57	2.87	2.04	2.48
Relative Accuracy (%)	6.3	15.9	8.8	10.6
Coefficient of Variation	0.030	0.076	0.042	0.051
Void Volume Percentage (%)	23.3 – 26.4	15.2 – 20.9	21.3 – 25.4	20.9 – 25.8

FINITE ELEMENT ANALYSIS OF A PULTRUDED THERMOPLASTIC COMPONENT

Many engineering designs cannot be solved with an exact solution at a set of specific initial and boundary conditions. In this case, a numerical approximation will often suffice for design purposes. Computer-aided FEA is used to numerically approximate and evaluate the response of a structural component under a load. FEA is performed by first dividing a component into discrete sections called elements. These elements are individually analyzed for stress and deflection at specific nodes. The results at the nodes are interpolated to obtain approximate values for areas between the nodes. FEA generally follows the schematic shown in Figure 37. The part geometry is typically generated using a computer-aided design (CAD) program. Element types and material properties are defined, and the geometry is meshed to define node locations. Boundary and loading conditions are defined, and the part is analyzed under these conditions. Results are then studied to determine if the part satisfies the design and failure criteria. The design changes and the analysis process is repeated until a solution is attained [32].



Figure 37. General steps to perform FEA.

FEA was conducted on a constant profile cross-section that is currently fabricated with aluminum to determine the feasibility of processing it by pultrusion using thermo-plastic composite materials. The component is used in a structural application where it is part of an assembly and must support a force of 556 N at rest. The thickness of the component varies over its cross-section as shown in Figure 38. For the purpose of this thesis, the component will be referred to hereafter as TPX.

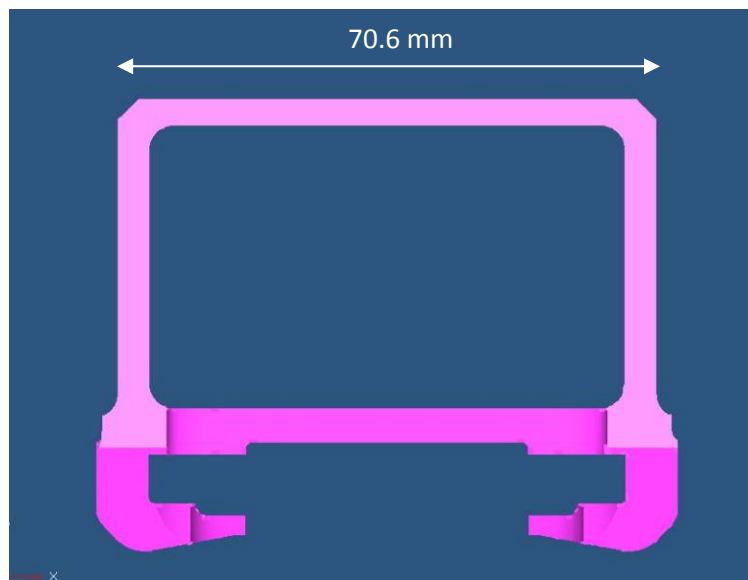


Figure 38. Cross-section of part geometry showing variable thickness.

The part geometry was re-drawn as a surface at the mid-plane so that the part could be analyzed as a laminated composite. The surface was imported into Altair Hypermesh 9.0. Hypermesh allows the user to mesh the surface using an ANSYS template (e.g. SOLID45, SHELL99) to define an element type to work specifically with the ANSYS program. The surface was meshed as a two-dimensional, quadrilateral mesh

with 19,472 elements. The element type was defined using the ANSYS template for a SHELL99 element.

The structural SHELL99 element is used for modeling composite laminates. Each lamina can be defined through the thickness of the part by specifying the location from the mid-plane, lamina thickness and the orientation angle of the fibers. Each element contains eight nodes that may translate in the x, y and z directions and rotate about the x, y and z axes. The mesh was imported into ANSYS 11.0 to perform the structural analysis.

Preliminary analysis was conducted on the aluminum component to verify that the model was working correctly. Values for the mass and deflection, along with the stress profiles, were compared to results previously obtained by the customer. The material properties used for the aluminum analysis are provided in Table 4.

Table 4

Properties of Aluminum 6061 used for FEA analysis of a TPX component

Properties of Aluminum 6061	
Density (kg/m ³)	2699
Ultimate Tensile Strength (MPa)	12.7
Tensile Yield Strength (MPa)	5.6
Modulus of Elasticity (GPa)	7.1
Poisson's Ratio	0.33
Shear Modulus (GPa)	2.7
Shear Strength (MPa)	8.4

Once the aluminum model was verified with results provided by the customer, FEA was performed by defining each layer (lamina) with a 0.508 mm thickness. The

maximum thickness of the component was 9.14 mm. As a result, a maximum number of eighteen layers were used. The cross-sectional thickness varies at different locations as shown in Figure 38. The SHELL99 element allows the user to drop (omit) layers in thinner areas of the part by defining them with a zero thickness. For the present analysis, Layers 1 – 4 were always defined with a 0.508 inch thickness, while Layers 5 – 9 were dropped in specific areas to yield the correct thicknesses. The composite can be defined as being symmetric about the mid-surface, so that only the layup sequence above the mid-surface needs to be defined. The position of the layers are shown in Figure 39.

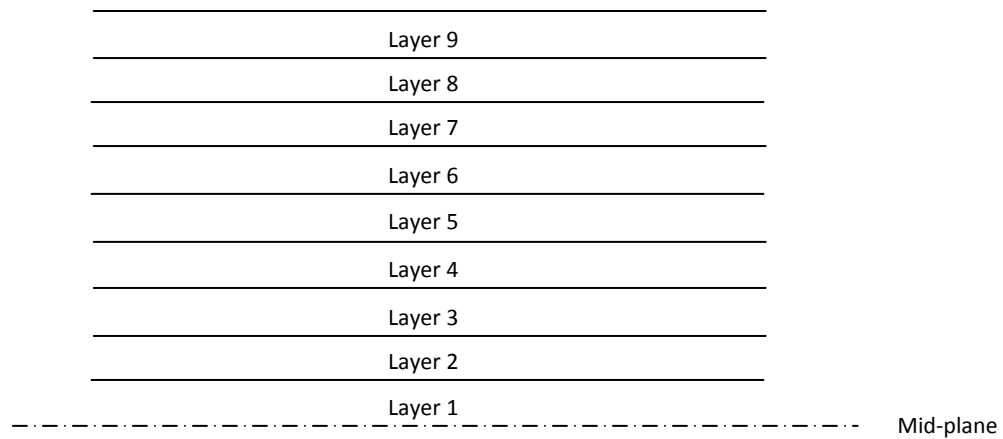


Figure 39. Position of layers with respect to the composite mid-plane.

The FEA for the laminate construction consisted of defining different layup sequences within the laminate. Carbon fiber impregnated with poly ether ether ketone resin (C/PEEK) with a fiber volume fraction of 58% was used in this analysis. The properties used are listed in Table 5 [33].

Table 5

Properties of carbon fiber impregnated with PEEK resin

Properties of C/PEEK	
Fiber Volume Fraction	0.58
Density (g/cm ³)	1.57
Longitudinal Tensile Strength (MPa)	2060
Transverse Tensile Strength (MPa)	78
Longitudinal Compressive Strength (MPa)	1100
Transverse Compressive Strength (MPa)	196
Longitudinal Modulus (GPa)	138
Transverse Modulus (GPa)	8.7
Major Poisson's Ratio	0.28
Minor Poisson's Ratio	0.2
In-plane Shear Modulus (GPa)	5.0
In-plane Shear Strength (MPa)	157

During operation, the TPX component is required to withstand 3558.6 N axially and in the downward direction (referred to as the negative y-direction from this point forward), as well as a 1334.5 N in the transverse direction. These forces were applied during the simulation as shown in Figure 40. Analysis was also performed for a combined loading of all three loads placed simultaneously. A constraint of zero deflection was placed at four bolt holes on each side of the component. The loading and constraint locations are shown in Figure 40.

FEA was first conducted on the existing aluminum component to provide a baseline. The deflection and stress values resulting from the loading scenarios fell within the specifications provided by the customer.

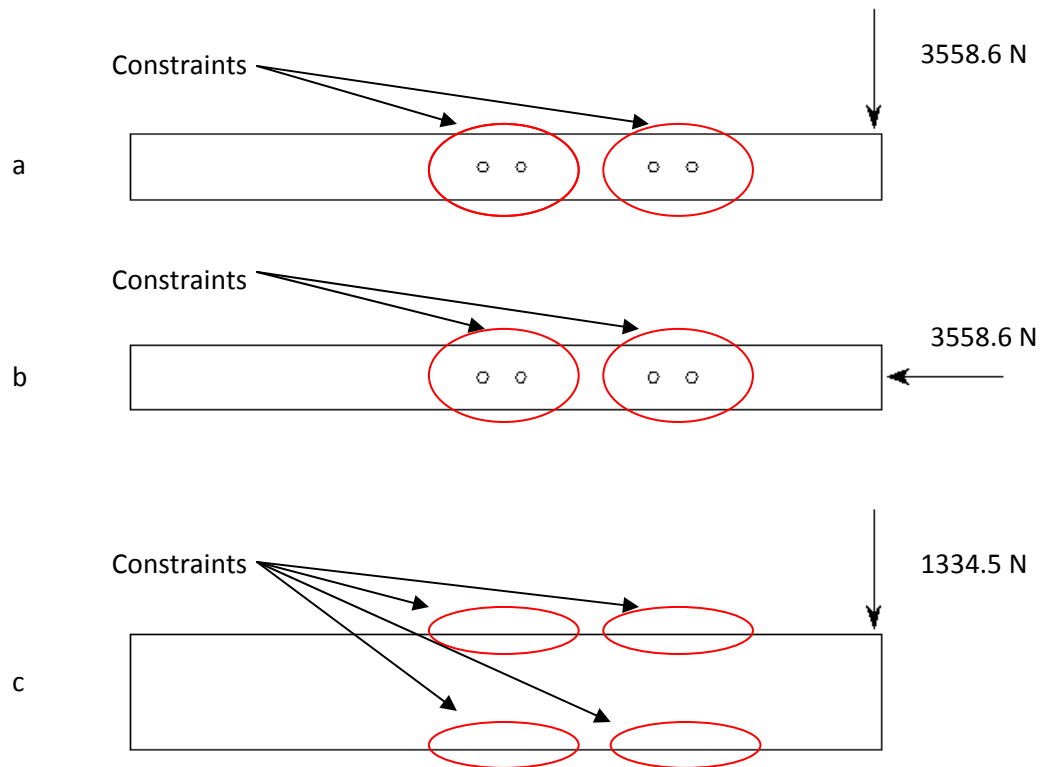


Figure 40. Forces and constraints applied to component TPX. Bolt holes circled in red were constrained for zero deflection a) side view of TPX component illustrating the 3558.6 N force in the negative y-direction b) side view of TPX component with 3558.6 N applied axially c) top view of component with 1334.5 N applied transversely.

Once the baseline was established, the part was analyzed using continuous, uni-directional C/PEEK material oriented at 0° . The maximum deflections were compared to the baseline and are shown in Table 6. The aluminum component deflected 46.8% more than the C/PEEK component when loaded axially. A unidirectional composite is strongest in the axial direction (parallel to the fibers), thus the results indicate that the composite part can outperform the aluminum part in the axial direction. The deflection of the aluminum component was 65.6% - 120.9% less than that of the C/PEEK component

when the transverse, negative y-direction and combined loading cases were applied.

Representative results of the axial loading are shown in Figure 41.

Table 6

Deflection of aluminum and C/PEEK unidirectional fiber components under different loading conditions

Loading	Aluminum Deflection (mm)	C/PEEK Deflection (mm)	Percent Difference
Axial (3558.6 N)	0.1194	0.0635	46.8
Negative y-direction (3558.6 N)	10.66	17.64	65.6
Transverse (1334.5 N)	9.571	21.04	120.9
Combined Axial, negative y-direction (3558.6 N) Transverse (1334.5 N)	15.78	27.31	73.1

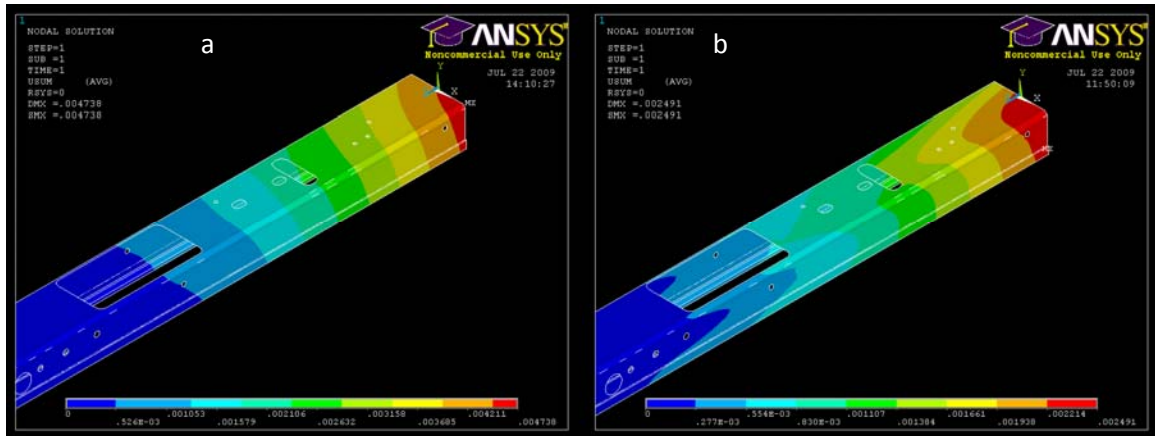


Figure 41. Deflection from 3558.6 N load in the axial direction on a) aluminum component; values range from 0 mm (blue) 0.1194 mm (red) b) C/PEEK continuous, uniaxial component; values range from 0 mm (blue) to 0.0635 mm (red).

The results in Figures 42 and 43 illustrate typical Von Mises stress distribution. The TPX component is loaded transversely in Figure 42, producing a maximum stress of 903 MPa at A of the TPX component. It is commonly known that transverse mechanical properties are significantly lower than longitudinal properties due to the anisotropy of composites [5]. Bending occurs at A, creating a compressive load in the bend as well as shear stresses between the fibers and matrix. The resulting bending stress of 903 MPa is 78.2% higher than the transverse compressive strength of 196MPa (also refer to Table 4).

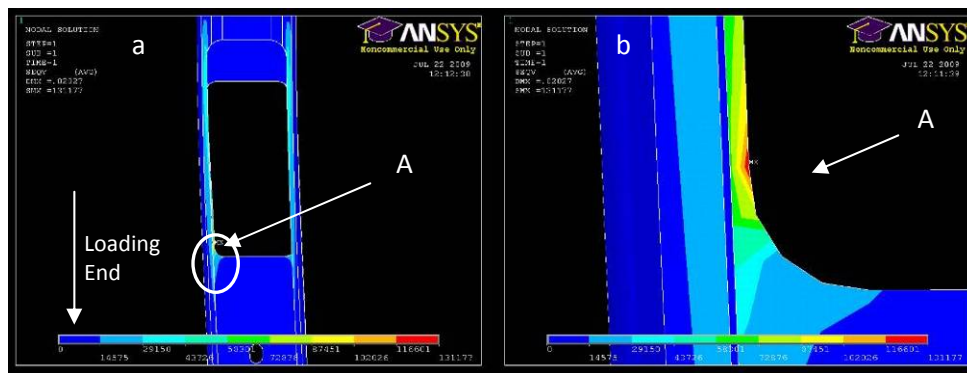


Figure 42. a) Von Mises stress distribution on upper portion of component from 1334.5 N applied transversely b) close-up view of maximum stress area; values range from 0 Pa (blue) – 9.03×10^8 Pa (red).

The combined loading (axial + transverse+ negative y-direction) analysis is shown in Figure 43. In this analysis, loads are applied to the component simultaneously. The loading created a combination of bending and torsion. A maximum stress of 132 GPa is located at the hole referred to as B in Figure 43, which is located nearest to the applied (combined) loads. The maximum combined stress of 132 GPa exceeds the transverse compression strength of 196 MPa for the material. This suggests that the stress

values can be reduced by incorporating selective fiber reinforcements to provide additional strength at this location.

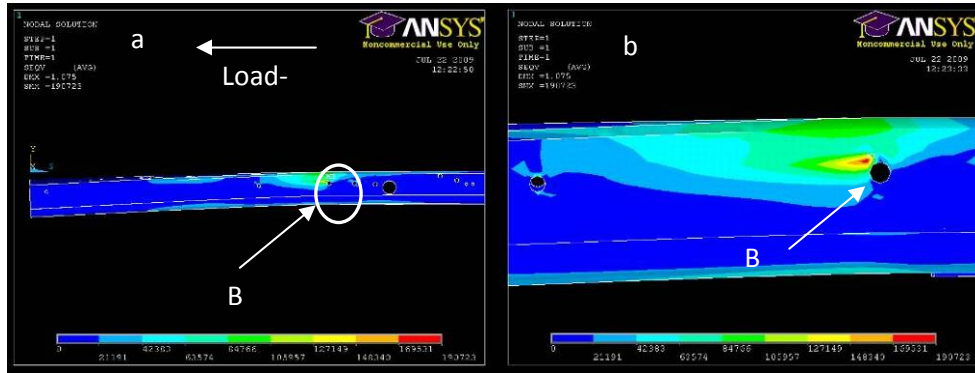


Figure 43. a) Von Mises stress distribution on side of component from 3558.6 N applied axially and in the negative y-direction and 1334.5 N applied transversely b) close-up view of maximum stress area; values range from 0 Pa (blue) – 1.32×10^9 Pa (red).

Table 7

Deflection values of various layup sequences of C/PEEK under different loading conditions

Layup orientation	Deflection axial (mm)	Deflection transverse (mm)	Deflection negative y (mm)	Deflection combined (mm)
$[0_6/-45/0/+45]_s$	0.1041	16.30	13.42	21.56
$[0_6/-45/+45/0]_s$	0.1041	16.28	13.53	21.74
$[0_5/+45/-45/0/0]_s$	0.1118	18.50	14.12	23.43
$[0_5/-45/0/+45/0]_s$	0.1067	13.86	18.21	23.00
$[0_7/+45/-45]_s$	0.1067	14.83	13.37	20.96
$[0_5/+45/+60/-60/-45]_s$	0.8712	42.21	45.36	66.68
$[+45/+60/-60/-45/0_5]_s$	0.0635	20.43	17.52	27.03
$[0_7/+60/-60]_s$	0.1092	15.49	13.52	22.21
$[0_7/+30/-30]_s$	0.0864	14.04	12.73	18.73

Axial loading exerts longitudinal compression in the part. Each layup sequence was analyzed while placed under axial loading. The $[0_7/+30/-30]_s$ sequence performs

better in deflection, deflecting 23.5% less than the $[0_7/+45/-45]_s$ sequence. The $\pm 30^\circ$ laminae are more capable of withstanding the axial loads than the $\pm 45^\circ$ laminae in axial loading because the fibers are aligned closer to the force direction. The largest differences occur for oriented laminae. This is the case with the $[0_5/+45/+60/-60/-45]_s$ which deflected 0.8712 mm, 908% more than the $[0_7/+30/-30]_s$ which deflected 0.0864 mm.

The deflections due to transverse loading varied from 14.83 mm to 42.21 mm. The $[0_5/-45/0/+45/0]_s$ and $[0_7/+30/-30]_s$ layup sequences performed better, deflecting 13.86 mm and 14.04 mm, respectively. The lowest deflection from a combined loading case results from the $[0_7/+30/-30]_s$ sequence, deflecting 11.9% less than the $[0_7/+45/-45]_s$ layup sequence. The deflections due to combined loading are shown in Figure 44 for these two layup orientations.

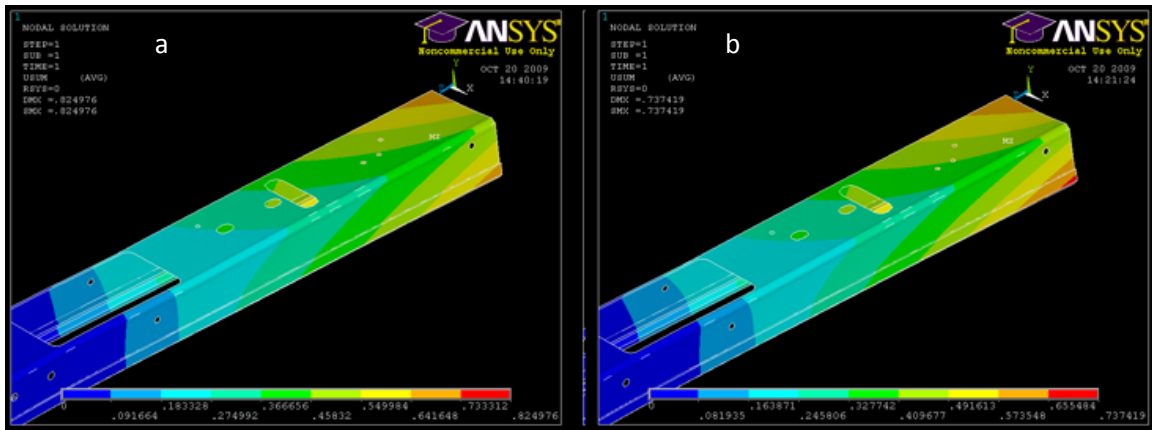


Figure 44. Deflections resulting from the combined loading scenario on a) $[0_7/45/-45]_s$ layup orientation; 20.96 mm deflection b) $[0_7/30/-30]_s$ layup orientation; 18.73 mm deflection.

Figures 45, 46, and 47 show the maximum stress locations that result from the combined loading case for the $[0_7/30/-30]_s$, $[0_7/45/-45]_s$ and $[0_7/60/-60]_s$ layup orientations. The maximum stress occurs at the location of the large cutout at the top of the part

in both the $[0_7/30/-30]_s$ and $[0_7/45/-45]_s$ sequences. The cutout produces a stress concentration. When the transverse load acts to bend the part, the maximum stress occurs at the corner of the cutout that is placed in tension.

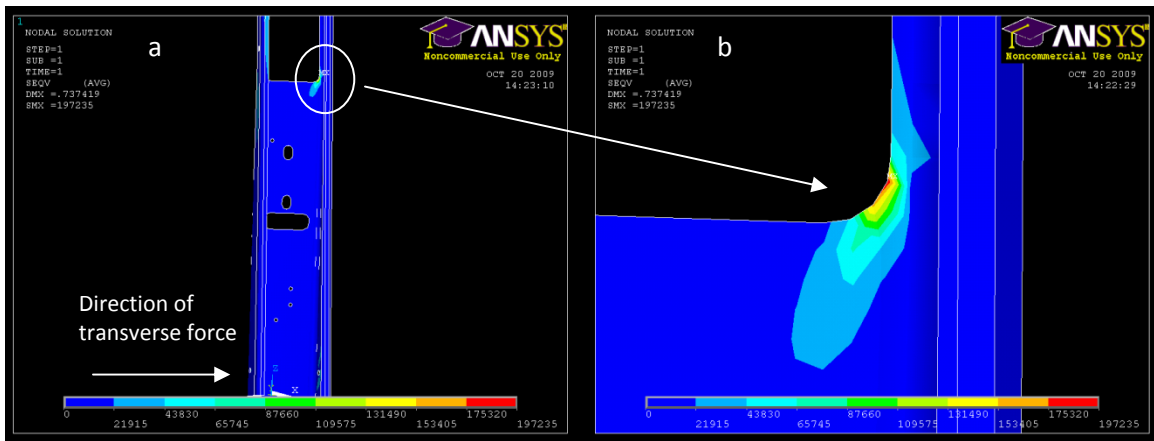


Figure 45. a) Von Mises stress resulting from combined loading scenario for $[0_7/30/-30]_s$ b) close-up of maximum stress area, 1.36×10^9 Pa.

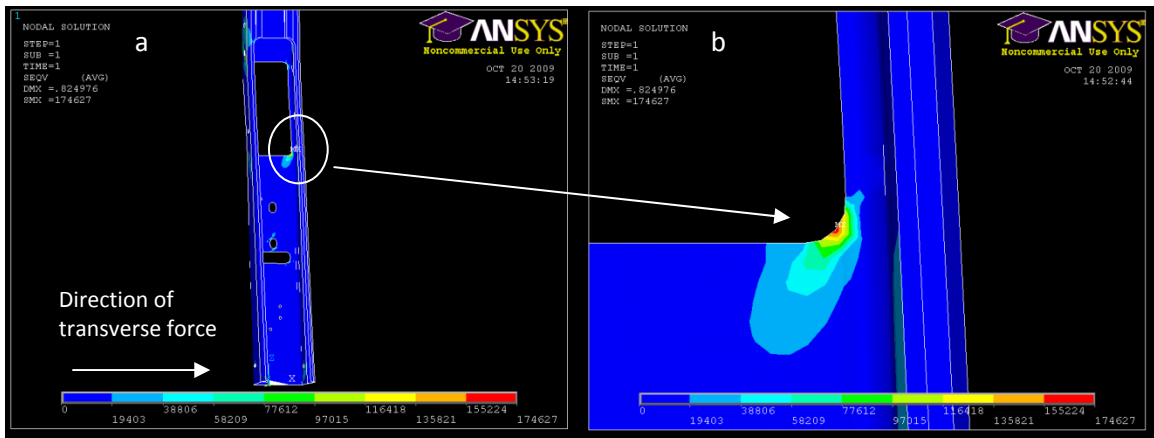


Figure 46. a) Von Mises stress resulting from combined loading scenario for $[0_7/45/-45]_s$ b) close-up of maximum stress area, 1.20×10^9 Pa.

The $[0_7/60/-60]_s$ layup sequence resulted in a different location of maximum stress. The constrained bolt hole closest to the loading end is placed under the highest stress. This occurs on the side that is placed in tension from the applied transverse force. This occurs on the side that is placed in tension from the applied transverse force. The change in location likely comes about from a higher shear stress resulting from the transverse load. Fiber orientations greater than 45° would increase the in-plane shear stress when the part is placed under a transverse load. Since shear is a matrix-dominated property, the part deflects more in this scenario. This, coupled with the out-of-plane shear, place a higher stress at the constraint location.

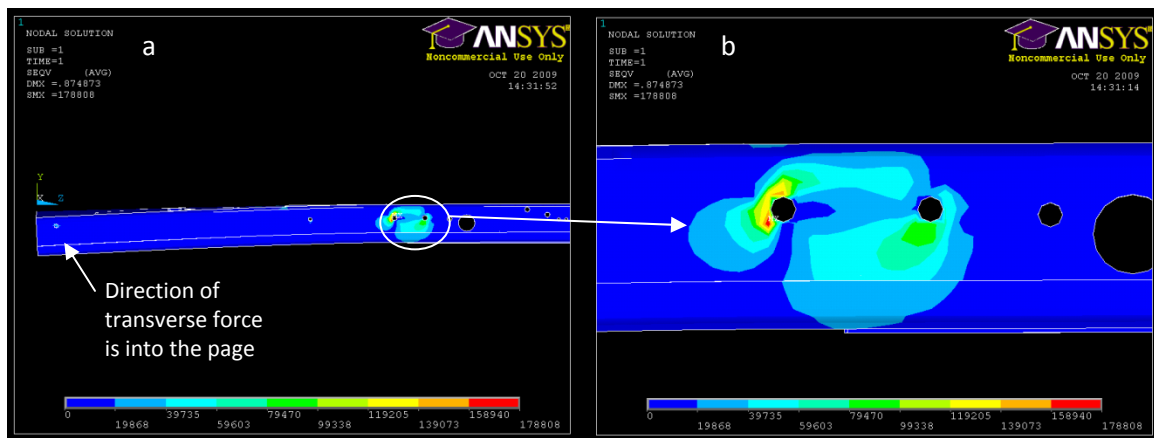


Figure 47. a) Von Mises stress resulting from combined loading scenario for $[0_7/60/-60]_s$ b) close-up of maximum stress area, 1.23×10^9 Pa.

The 0° layup sequence in this study allowed 72.8% more deflection than the existing aluminum component. By incorporating different angle orientations, the deflection values were decreased. The $[0_7/30/-30]_s$ layup sequence resulted in the lowest deflection values. The combined loading scenario produced a 15.75% higher deflection than occurred with the aluminum part, indicating that the angle orientation did not altogether

correct deflection from out-of-plane loading. The results highlight the need for additional geometric stiffening of the TPX component to limit the deflection that results from out-of-plane bending. Geometric stiffening, outside the scope of this work, can be incorporated into the component design in the form of selectively placed ribs.

CONCLUSIONS

A thermoset pultrusion apparatus was modified to process thermoplastic materials. This was accomplished by incorporating a pre-heater, guidance system, and a new die assembly. A parametric study was then performed using the modified system to determine a processing window for commingled tows. A study was performed to determine the effect of temperature on the line speed. The results showed a 0.96% decrease in line speed when the temperature was increased from 215°C to 221°C. Further increasing the temperature from 221°C to 227°C resulted in a line speed increase of 1.1%. These results were helpful in determining the resin behavior at the temperatures to be studied. The decrease in line speed at 221°C indicates a pressure increase brought about from an increase in the resin backflow. The line speed increase occurring at 227°C indicates a decrease in resin viscosity, which can facilitate fiber wet-out.

Mechanical testing was performed to determine which properties produced a composite with the highest mechanical properties. Flexure testing showed that a temperature of 221°C produced the highest flexural strength at 232.4 MPa. The properties of the material processed at 227°C and 232°C is an average of 1.6% lower than the material pultruded at 221°C. ILSS testing showed that the highest short-beam strength (16.1 MPa) occurred for the material processed at 221°C. The material pultruded at 215°C and 232°C resulted in short-beam strengths of 15.7 MPa and 15.5 MPa, an average 1.9%

lower than the highest strength. The lowest short-beam strength (14.9 MPa) occurred for the processing temperature of 227°C, 8.1% lower than the highest strength.

The material pultruded with 105 tows exhibited flexural properties that were 23.9% higher than material containing 100 tows and 55.8% higher than the material containing 95 tows. The ILSS results followed this trend, as well, with a short-beam shear strength of 14.9 MPa for 105 tows, 16.4% lower (12.8 MPa) for 100 tows and 35.6% lower (11.0 MPa) for 95 tows. This is attributed to an increase in fiber content as well as pressure within the die that occurs with increasing the tow number.

Increasing line speeds decrease the residence time of the material in the heating die, which affects both resin flow and pressure. Flexural strength was highest for the material processed at 254 mm/min (228.5 MPa) and 508 mm/min (226.7 MPa). The lowest properties occurred for the material produced at 381 mm/min (180.3 MPa) and 635 mm/min (183.2 MPa). These results indicate the interdependency of the processing parameters. The material pultruded at 254 mm/min had a longer residence time within the die, which resulted in better polymer melting and flow. The higher line speed, 508 mm/min, decreases the heating time of the polymer. The faster pulling speed coupled with the resulting higher resin viscosity creates a higher pressure as the material moves through the die. The lowest strengths are 180.3 MPa for a line speed of 381 mm/min and 183.2 MPa for a line speed of 635 mm/min. Processing at a line speed of 381 mm/min seems to provide insufficient resin melt time, while failing to produce a large enough backflow pressure to consolidate the high viscosity resin. Material processed at 635 mm/min did not allow sufficient resin melt time to lower the polymer viscosity and allow flow. The ILSS results show that a line speed of 318 mm/min yields the highest short-

beam shear strength of 15.5 MPa. The lowest short-beam shear strength (13.68 MPa), occurs for a line speed of 635 mm/min and is 12.3% higher than the strength at a line speed of 318 mm/min.

The void volume percentage was determined for the composites produced in the temperature and tow studies to compare the microstructure to the results for the mechanical testing. The lowest percentage of voids (21.3 – 25.4%) in the tow study occurred for the material containing 105 tows. This supports the mechanical testing results which show that the highest properties occur for the material with the highest tow number. The increase in material volume decreased the number of voids that can lower the composite's mechanical properties. The highest void percentage (38.2 – 44.9%) occurred for the material pultruded with 95 tows, explaining the property decrease with decreasing tow number.

The processing temperature that resulted in the least number of voids was 221°C, producing a 15.2 – 20.9% void volume percentage. This sample yielded the highest test results in both flexure and ILSS testing. The minimum void volume coupled with the mechanical testing results indicate that of the temperatures studied, a processing temperature of 221°C produces the highest quality pultruded component using this material system.

FEA analysis indicated that a 0° composite resulted in deflection values 72.8% higher for combined loading (axial, negative y and transverse) than the aluminum component. Angle orientations were selected to decrease the deflection by balancing the bending and torsional stresses that occur from loading. Of the layup sequences studied, $[0_7/30/-30]_s$ and $[0_7/45/-45]_s$ improved the strength and stability of the component by stif-

fening the component and decreasing the deflection. The lowest deflection value for the combined loading scenario resulted from the $[0_7/30/-30]_s$ layup sequence, however, out-of-plane bending continue to allow a deflection 15.75% higher than the baseline component. Geometric stiffening can be incorporated into the design easily to further reduce the component deflection.

The benefits that thermoplastic resins afford greatly outweigh the processing challenges presented by their high melt viscosities. The thermoplastic pultrusion method has shown itself to be highly adaptable to a wide variety of applications. The desired properties can be easily modified to suit individual customer specifications, such as increased axial and bending stiffness. The most practical benefit to industry is the low cost of production when compared to other composite processing methods.

FUTURE WORK

The advantages of processing thermoplastic resins using the pultrusion method will provide motivation to conduct further research. The current pultrusion apparatus design can be used to process a variety of other thermoplastic resins. Additional material forms, including hot-melt impregnated tape and higher resin content prepregs, will also be processed to determine which form provides the best overall composite properties. Research can be expanded to include multidirectional fabrics and mats. This adaptation will allow for a greater variety of angle orientations and mechanical properties, which in turn will broaden the range of applications for which this process can be used.

The current FEA analysis indicates that the component requires some geometric stiffening to decrease deflection during static loading. Future analysis will include dynamic analysis using LS-DYNA to determine the amount of deflection due to dynamic loading. Once these values are determined, the component design will be modified to incorporate geometric stiffening in the form of ribs. The design modification will be analyzed in both ANSYS and LS-DYNA to ensure that the amount of deflection falls within the range of the existing aluminum component.

REFERENCES

1. Schwartz, M.M., *Composite Materials: Properties, Nondestructive Testing and Repair*. Vol. I. 1997, Upper Saddle River: Prentice Hall PTR.
2. Starr, T.F., *Pultrusion for Engineers*. 2000, Cambridge: Woodhead Publishing Limited.
3. Schwartz, M.M., *Composite Materials: Processing, Fabrication and Applications*. Vol. II. 1997, Upper Saddle River: Prentice Hall PTR.
4. Bernhardt, E.C., *Processing of Thermoplastic Materials*. SPE Plastics Engineering Series. 1959, New York: Reinhold Publishing Corporation.
5. Mallick, P.K., *Fiber-reinforced composites: materials, manufacturing and design*. Second ed. 1993, New York: CRC Press.
6. Cho, B.-G., et al., *Fiber reinforced Nylon-6 composites produced by the reaction injection pultrusion process*. *Polymer Composites*, 1996. **17**(5): p. 673-681.
7. Velde, K.V.d. and P. Kickens, *Thermoplastic pultrusion of natural fibre reinforced composites*. *Composite Structures*, 2001. **54**: p. 355-360.
8. Miller, A.H., et al., *High speed pultrusion of thermoplastic matrix composites*. *Composites: Part: A*, 1998. **2**: p. 773-782.
9. Sala, G. and D. Cutolo, *The pultrusion of powder-impregnated thermoplastic composites*. *Composites: Part A*, 1997. **28A**: p. 637-646.

10. Haffner, S.M., et al., *Finite-element-assisted modelling of a thermoplastic pultrusion process for powder-impregnated yarn*. Composites Science and Technology, 1998. **58**: p. 1371-1379.
11. Ma, C.-C.M., et al., *Processing and properties of pultruded thermoplastic composites (I)*. Composites Manufacturing, 1990. **1**(3): p. 191-196.
12. Nejhad, M.N.G., *Thermal analysis for thermoplastic composites tow/tape pre-heating and pultrusion*. Journal of Thermoplastic Composite Materials, 1997. **10**: p. 1997.
13. Borazghi, H., et al., *Continuous consolidation of polypropylene/glass fiber commingled fabric*. Polymers and Polymer Composites, 2008. **16**(1): p. 1-8.
14. Akovali, G., *Handbook of Composite Fabrication*. 2001, Shawbury: Rapra Technology Limited.
15. Kim, D.-H., W.I. Lee, and K. Friedrich, *A model for a thermoplastic pultrusion process using commingled yarns*. Composites Science and Technology, 2001. **61**: p. 1065-1077.
16. Chang, I.Y. and J.K. Lees, *Recent development in thermoplastic composites: A review of matrix systems and processing methods*. Journal of Thermoplastic Composite Materials, 1988. **1**: p. 277-296.
17. Mallick, P.K., *Composites Engineering Handbook*. 1997, New York: Marcel Dekker, Inc.
18. Kerbirou, V. and K. Friedrich, *Pultrusion of thermoplastic composites - Process optimization and mathematical modeling*. Journal of Thermoplastic Composite Materials, 1999. **12**: p. 96-120.

19. Chhabra, R.P. and J.F. Richardson, *Non-Newtonian Flow: Fundamentals and Engineering Applications*. 1999, Oxford: Butterworth-Heinemann.
20. Hepola, P.J., *Thermoplastic Pultrusion with On-line Dry Powder Impregnation of Fibers*, in *Mechanical Engineering*. Fall 1993, University of Delaware. p. 213.
21. Wilkinson, W.L., *Non-Newtonian Fluids: Fluid Mechanics, Mixing and Heat Transfer*. 1960, London: Pergamon Press.
22. Advani, S.G. and E.M. Sozer, *Process Modeling in Composite Manufacturing*. 2002, New York: CRC Press.
23. Lee, W.I. and G.S. Springer, *A model of the manufacturing process of thermoplastic matrix composites*. *Journal of Composite Materials*, 1987. **21**: p. 1017-1053.
24. Astrom, B.T., R.B. Pipes, and S.G. Advani, *On Flow through Aligned Fiber Beds and Its Application to Composites Processing*. *Journal of Composite Materials*, 1992. **26**(9): p. 1351-1373.
25. Åström, B.T., P.H. Larsson, and R.B. Pipes, *Development of a facility for pultrusion of thermoplastic-matrix composites*. *Composites Manufacturing*, 1991. **2**(2): p. 114-123.
26. Wiedmer, S. and M. Manolesos, *Experimental study of the pultrusion of carbon fiber - Polyamide 12 yarn*. *Journal of Thermoplastic Composite Materials*, 2006. **19**: p. 97-111.
27. Hodgkinson, J.M., *Mechanical Testing of Advanced Fibre Composites*. 2000, Cambridge, England: Woodhead Publishing Limited.

28. Kamble, V.D., *Optimization of Thermoplastic Pultrusion Process Using Commingled Fibers*, in *Materials Science and Engineering*. 2008, University of Alabama at Birmingham: Birmingham.
29. Lee, W.I. and G.S. Springer, *Pultrusion of thermoplastics - A model*. *Journal of Composite Materials*, 1991. **25**: p. 1632-1652.
30. Davis, J.R., *Surface Engineering for Corrosion and Wear Resistance*. 2001, Materials Park: ASM International.
31. Agarwal, B.D., L.J. Broutman, and K. Chandrashekhara, *Analysis and Performance of Fiber Composites, 3rd Edition*. 2006, Hoboken: Wiley.
32. Hutton, D.V., *Fundamentals of Finite Element Analysis*. 2003, New York: McGraw Hill.
33. Daniel, I.M. and O. Ishai, *Engineering Mechanics of Composite Materials*. 2nd ed. 2006, New York: Oxford University Press.

APPENDIX A
THERMAL ANALYSIS DATA

Sample: Twintex
Size: 0.1500 mg

DSC

File: Twintex.001
Operator: Leigh
Run Date: 24-Sep-2008 10:53

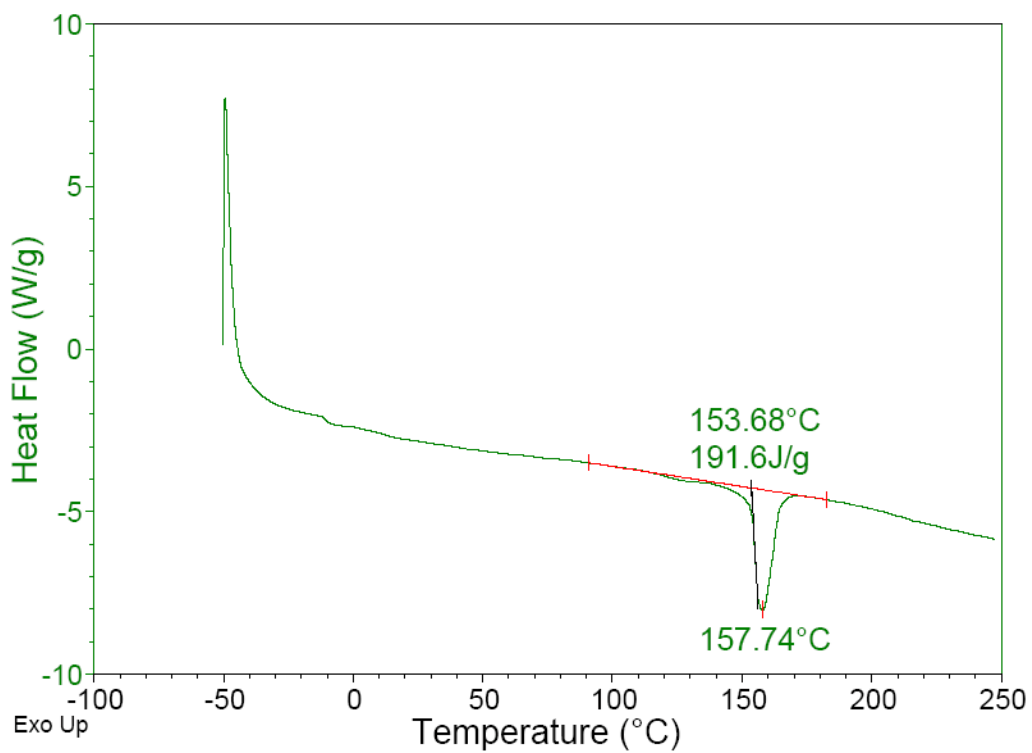


Figure A-1. DSC results for Twintex® E-glass/PP commingled tows identifying the melting temperature of the matrix, which is observed to be 157.74°C.

APPENDIX B

INTERLAMINAR SHEAR STRENGTH TEST DATA

Table B-1

Dimensions of 95 tow sample for ILSS testing

Specimen Number	Midsection Width (mm)	Midsection Thickness (mm)	Length (mm)
1	8.10	4.24	26.53
2	8.68	4.29	25.29
3	8.78	4.24	26.49
4	8.45	4.24	26.67
5	8.68	4.30	26.53

Table B-2

Dimensions of 100 tow sample for ILSS testing

Specimen Number	Midsection Width (mm)	Midsection Thickness (mm)	Length (mm)
1	8.94	4.24	26.53
2	8.71	4.29	25.29
3	8.91	4.24	26.49
4	8.38	4.24	26.67
5	8.83	4.30	26.53

Table B-3

Dimensions of 420°C sample for ILSS testing

Specimen Number	Midsection Width (mm)	Midsection Thickness (mm)	Length (mm)
1	8.81	4.24	26.56
2	8.48	4.34	25.98
3	8.96	4.26	26.31
4	8.71	4.25	26.42
5	8.86	4.21	26.46

Table B-4

Dimensions of 430°C sample for ILSS testing

Specimen Number	Midsection Width (mm)	Midsection Thickness (mm)	Length (mm)
1	8.96	4.19	26.31
2	8.61	4.31	26.51
3	8.38	4.36	25.90
4	8.91	4.25	26.00
5	8.82	4.21	26.42

Table B-5

Dimensions of 440°C sample for ILSS testing

Specimen Number	Midsection Width (mm)	Midsection Thickness (mm)	Length (mm)
1	8.58	4.33	26.44
2	8.53	4.34	26.36
3	8.66	4.24	27.43
4	8.50	4.31	26.21
5	8.58	4.19	26.86

Table B-6

Dimensions of 450°C sample for ILSS testing

Specimen Number	Midsection Width (mm)	Midsection Thickness (mm)	Length (mm)
1	8.89	4.21	26.21
2	8.68	4.26	25.32
3	8.94	4.25	24.57
4	8.17	4.26	24.86
5	8.83	4.25	26.31

Table B-7

Dimensions of 381 mm/min sample for ILSS testing

Specimen Number	Midsection Width (mm)	Midsection Thickness (mm)	Length (mm)
1	8.17	4.29	26.06
2	8.58	4.15	25.83
3	9.04	4.20	25.89
4	8.63	4.16	25.66
5	8.72	4.27	25.98

Table B-8

Dimensions of 508 mm/min sample for ILSS testing

Specimen Number	Midsection Width (mm)	Midsection Thickness (mm)	Length (mm)
1	8.43	4.26	25.92
2	8.30	4.26	25.60
3	8.25	4.14	26.28
4	8.38	4.34	26.08
5	9.42	4.16	25.40

Table B-9

Dimensions of 635 mm/min sample for ILSS testing

Specimen Number	Midsection Width (mm)	Midsection Thickness (mm)	Length (mm)
1	8.53	4.17	25.53
2	8.76	4.39	25.05
3	8.78	4.26	26.67
4	8.58	4.31	24.95
5	8.62	4.34	25.71

Table B-10

Statistical analysis for ILSS testing of temperature samples

Temperature (°C)	215	221	227	232
Mean, X	15.75	16.1	15.2	15.7
Standard Deviation	0.569	0.601	1.97	0.901
Coefficient of Variation	3.61	3.74	12.9	5.74

Table B-11

Statistical analysis for ILSS testing of tow samples.

Tow Number	95 tows	100 tows	105 tows
Mean, X	15.5	12.8	15.2
Standard Deviation	0.946	0.445	1.97
Coefficient of Variation	6.11	3.49	12.9

Table B-12

Statistical analysis for ILSS testing of line speed samples

Line Speed (mm/min)	254	381	508	635
Mean, X	15.2	15.5	14.5	13.7
Standard Deviation	1.97	0.946	0.437	0.797
Coefficient of Variation	12.9	6.11	3.02	5.81

APPENDIX C
VOID VOLUME FRACTION DATA

Table C-1

Point count data for 95 tow material processed at 227°C

Image	Point Count, P_p	Individual Point Count, $P_p(i)$
1	17.5	0.313
2	18	0.321
3	13	0.232
4	15.5	0.277
5	19	0.339
6	19	0.339
7	20.5	0.366
8	18	0.321
9	22.5	0.402
10	20	0.357
11	17	0.304
12	16	0.286
13	19	0.339
14	19.5	0.348
15	17.5	0.313
16	20	0.357
17	18	0.321
18	20.5	0.366
19	20	0.357
20	28.5	0.330

Table C-2

Point count data for 100 tow material processed at 227°C

Image	Point Count, P_p	Individual Point Count, $P_p(i)$
1	20.5	0.366
2	18	0.321
3	14	0.250
4	12	0.330
5	14	0.250
6	18.5	0.330
7	17.5	0.313
8	17	0.304
9	19	0.339
10	17.5	0.313
11	13.5	0.241
12	9.5	0.170
13	15	0.268
14	16	0.286
15	18	0.321
16	19	0.339
17	13.5	0.241
18	15	0.268
19	21	0.375
20	13	0.232

Table C-3

Point count for 105 tow material processed at 227°C

Image	Point Count, P_p	Individual Point Count, $P_p(i)$
1	10	0.179
2	10.5	0.188
3	12	0.214
4	9.5	0.170
5	13.5	0.241
6	10	0.179
7	14.5	0.259
8	14.5	0.259
9	17.5	0.313
10	13.5	0.241
11	12	0.214
12	14.5	0.259
13	17	0.304
14	12	0.214
15	13	0.232
16	15.5	0.277
17	9.5	0.170
18	16	0.286
19	14.5	0.259
20	12	0.214

Table C-4

Point count for material processed at 215°C

Image	Point Count, P_p	Individual Point Count, $P_p(i)$
1	14.5	0.259
2	13	0.232
3	15	0.268
4	13	0.232
5	15	0.277
6	11	0.169
7	16	0.286
8	11.5	0.205
9	11.5	0.205
10	15.5	0.277
11	14	0.250
12	13	0.232
13	14	0.250
14	14.5	0.259
15	13.5	0.241
16	12.5	0.223
17	12	0.214
18	14	0.250
19	15	0.268
20	19	0.339

Table C-5

Point count for material processed at 221°C

Image	Point Count, P_p	Individual Point Count, $P_p(i)$
1	10.5	0.188
2	9.9	0.177
3	7.5	0.134
4	11	0.196
5	10.5	0.188
6	10	0.179
7	9	0.161
8	6	0.107
9	7	0.125
10	6	0.107
11	15.5	0.277
12	11	0.196
13	10.5	0.188
14	18	0.321
15	7.5	0.134
16	7.5	0.134
17	5	0.089
18	14	0.250
19	15	0.268
20	11	0.196

Table C-6

Point count for material processed at 227°C

Image	Point Count, P_p	Individual Point Count, $P_p(i)$
1	12.5	0.223
2	14	0.250
3	13	0.232
4	15	0.268
5	9.5	0.170
6	8	0.143
7	16	0.286
8	12	0.214
9	15	0.268
10	19	0.339
11	13	0.232
12	11.5	0.205
13	15.5	0.277
14	11.5	0.205
15	13.5	0.241
16	8	0.143
17	10	0.179
18	13	0.232
19	18.5	0.330
20	13	0.232